

1  
AFCRL-TR-75-0616 ✓  
INSTRUMENTATION PAPERS, NO. 243 ✓

12



g

ADA022673

# Design Criteria and Numerical Simulation of an Antenna System for One-Dimensional Limited Scan

GIORGIO V. BORGIOTTI

DDC  
RECEIVED  
APR 6 1976  
REGISTERED

27 C

2 December 1975

Approved for public release; distribution unlimited.

MICROWAVE PHYSICS LABORATORY PROJECT 4600  
AIR FORCE CAMBRIDGE RESEARCH LABORATORIES  
HANSCOM AFB, MASSACHUSETTS 01731

AIR FORCE SYSTEMS COMMAND, USAF



Qualified requestors may obtain additional copies from the Defense Documentation Center. All others should apply to the National Technical Information Service.

ACQUISITION FOR	
NTIS	White Section <input checked="" type="checkbox"/>
DIC	Ext. Section <input type="checkbox"/>
UWL	<input type="checkbox"/>
JUSTIFICATION	
BY	
DISTRIBUTION AVAILABILITY CODES	
DRM	AVAIL. CODE OR SPECIAL
A	

9 Instrumentation papers, #

Unclassified

SECURITY CLASSIFICATION OF THIS PAGE (When Data Entered)

REPORT DOCUMENTATION PAGE		READ INSTRUCTIONS BEFORE COMPLETING FORM	
1. REPORT NUMBER AFCL-TR-75-0616, AFCL-IP-243	2. GOVT ACCESSION NO.	3. RECIPIENT'S CATALOG NUMBER	
4. TITLE (and Subtitle) DESIGN CRITERIA AND NUMERICAL SIMULATION OF AN ANTENNA SYSTEM FOR ONE-DIMENSIONAL LIMITED SCAN.		5. TYPE OF REPORT & PERIOD COVERED Scientific. Interim.	
7. AUTHOR(s) Giorgio V. Borgiotti		6. PERFORMING ORG. REPORT NUMBER IP No. 243	
		8. CONTRACT OR GRANT NUMBER(s)	
9. PERFORMING ORGANIZATION NAME AND ADDRESS Air Force Cambridge Research Laboratories (LZR) Hanscom AFB Massachusetts 01731		10. PROGRAM ELEMENT, PROJECT, TASK AREA & WORK UNIT NUMBERS 46001303 62702F	
11. CONTROLLING OFFICE NAME AND ADDRESS Air Force Cambridge Research Laboratories (LZR) Hanscom AFB Massachusetts 01731		12. REPORT DATE 2 December 1975	
		13. NUMBER OF PAGES 64	
14. MONITORING AGENCY NAME & ADDRESS (if different from Controlling Office) AF-4600, 460013		15. SECURITY CLASS. (of this report) Unclassified	
		15a. DECLASSIFICATION/DOWNGRADING SCHEDULE	
16. DISTRIBUTION STATEMENT (of this Report) Approved for public release; distribution unlimited. 12 64 p.			
17. DISTRIBUTION STATEMENT (of the abstract entered in Block 20, if different from Report)			
18. SUPPLEMENTARY NOTES This research was accomplished while the author held a National Research Council Resident Senior Research Associateship.			
19. KEY WORDS (Continue on reverse side if necessary and identify by block number) Limited scan arrays Antenna systems Phased arrays Antenna theory			
20. ABSTRACT (Continue on reverse side if necessary and identify by block number) An analytical and numerical study was performed on a novel design scheme for an antenna system for limited one-dimensional scan. The system has a number of control elements approximately equal to the minimum that are theoretically compatible with the aperture size and field of view (FOV). The radiating structure consists of a "boot lace" lens with linear outer and circular inner profiles. This geometry plays a basic role in determining excellent scan performance over a moderate frequency band. A linear array whose size			

011800-16

cont

Unclassified

SECURITY CLASSIFICATION OF THIS PAGE(When Data Entered)

20. (Cont.)

depends critically upon scan requirements and the lens focal length is located on the focal plane and is focussed onto the inner lens profile. The array is fed by a Hybrid Network (HN) performing a spatial Fourier transformation. The input ports of the HN are fed by the output ports of a Beam Forming Network (BFN) through a set of variable phase shifters. The BFN has separate input ports for the sum and difference patterns controlled independently. The system works as follows. The antenna illumination is synthesized as the weighted superposition of components illuminations or "overlapping subarrays", each of which is due to the excitation of one of the ports of the HN. The amplitudes of the subarray excitations are fixed and determined by the power divisions provided by the BFN. Their phases are controlled by the set of variable phase shifters. A desirable feature of the scheme is that for fixed phase shifter settings, neither the beam scans nor the width changes for a moderate frequency variation. Through a suitable design of the BFN, ultralow sidelobes outside the FOV can be achieved at the expense of a slight reduction of the illumination efficiency, which is always high, however, since the aperture is fully used. Extensive numerical computations for an antenna having a half-power beamwidth of  $1.2^\circ$  shows that the sum beam can be scanned in a sector greater than 6 beams on a band of 20 percent with excellent performance from the viewpoint of gain and sidelobes, the scan sector being slightly less for the difference beam.

Unclassified

SECURITY CLASSIFICATION OF THIS PAGE(When Data Entered)

## Contents

1. INTRODUCTION	7
2. THE OVERLAPPING SUBARRAY CONCEPT	9
3. ANTENNA CONFIGURATION AND ANALYTICAL MODEL	11
4. THEORY OF OPERATION	15
5. DESIGN PROCEDURE AND COMPUTER SIMULATION OF A PARTICULAR CASE	18
6. NUMERICAL RESULTS AND DISCUSSION	20
7. CONCLUSIONS	53
REFERENCES	55
APPENDIX A: A Hybrid Network with a Number of Input Ports Twice the Number of the Output Ports	57
APPENDIX B: The Effects of Phase Quantization on Radiation Pattern	61

## Illustrations

1. Antenna System Scheme	12
2. Beam Forming Network for Independent Control of Sum and Difference Patterns	13
3. Amplitude and Phase Illumination of Subarray 1R, Frequency $f_0$	23
4. Radiation Pattern of Subarray 1R, Frequency $f_0$	23
5. Amplitude and Phase Illumination of Subarray 4T, Frequency $f_0$	24
6. Radiation Pattern of Subarray 4R, Frequency $f_0$	24
7. Sum Pattern, Amplitude and Phase Illumination; Scan Angle $\theta_0 = 0^\circ$ , Frequency $f_0$	25
8. Sum Pattern; Scan Angle $\theta_0 = 0^\circ$ , Frequency $f_0$	25
9. Sum Pattern, Amplitude and Phase Illumination; Scan Angle $\theta_0 = 1.2^\circ$ , Frequency $f_0$	26
10. Sum Pattern; Scan Angle $\theta_0 = 1.2^\circ$ , Frequency $f_0$	26
11. Sum Pattern, Amplitude and Phase Illumination; Scan Angle $\theta_0 = 2.4^\circ$ , Frequency $f_0$	27
12. Sum Pattern; Scan Angle $\theta_0 = 2.4^\circ$ , Frequency $f_0$	27
13. Sum Pattern, Amplitude and Phase Illumination; Scan Angle $\theta_0 = 3.6^\circ$ , Frequency $f_0$	28
14. Sum Pattern; Scan Angle $\theta_0 = 3.6^\circ$ , Frequency $f_0$	28
15. Difference Pattern, Amplitude and Phase Illumination; Scan Angle $\theta_0 = 0^\circ$ , Frequency $f_0$	29
16. Difference Pattern; Scan Angle $\theta_0 = 0^\circ$ , Frequency $f_0$	29
17. Difference Pattern, Amplitude and Phase Illumination; Scan Angle $\theta_0 = 1.2^\circ$ , Frequency $f_0$	30
18. Difference Pattern; Scan Angle $\theta_0 = 1.2^\circ$ , Frequency $f_0$	30
19. Difference Pattern, Amplitude and Phase Illumination; Scan Angle $\theta_0 = 2.4^\circ$ , Frequency $f_0$	31
20. Difference Pattern; Scan Angle $\theta_0 = 2.4^\circ$ , Frequency $f_0$	31
21. Difference Pattern, Amplitude and Phase Illumination; Scan Angle $\theta_0 = 3.6^\circ$ , Frequency $f_0$	32
22. Difference Pattern; Scan Angle $\theta_0 = 3.6^\circ$ , Frequency $f_0$	32
23. Amplitude and Phase Illumination of Subarray 1R, Frequency $0.9 f_0$	33
24. Radiation Pattern of Subarray 1R, Frequency $0.9 f_0$	33
25. Amplitude and Phase Illumination of Subarray 4R, Frequency $0.9 f_0$	34
26. Radiation Pattern of Subarray 4R, Frequency $0.9 f_0$	34
27. Sum Pattern Amplitude and Phase Illumination; Scan Angle $\theta_0 = 0^\circ$ , Frequency $0.9 f_0$	35
28. Sum Pattern; Scan Angle $\theta_0 = 0^\circ$ , Frequency $0.9 f_0$	35

## Illustrations

29. Sum Pattern, Amplitude and Phase Illumination; Scan Angle $\theta_0 = 1.2^\circ$ , Frequency $0.9 f_0$	36
30. Sum Pattern; Scan Angle $\theta_0 = 1.2^\circ$ , Frequency $0.9 f_0$	36
31. Sum Pattern, Amplitude and Phase Illumination; Scan Angle $\theta_0 = 2.4^\circ$ , Frequency $0.9 f_0$	37
32. Sum Pattern; Scan Angle $\theta_0 = 2.4^\circ$ , Frequency $0.9 f_0$	37
33. Sum Pattern, Amplitude and Phase; Scan Angle $\theta_0 = 3.6^\circ$ , Frequency $0.9 f_0$	38
34. Sum Pattern; Scan Angle $\theta_0 = 3.6^\circ$ , Frequency $0.9 f_0$	38
35. Difference Pattern, Amplitude and Phase Illumination; Scan Angle $\theta_0 = 0^\circ$ , Frequency $0.9 f_0$	39
36. Difference Pattern; Scan Angle $\theta_0 = 0^\circ$ , Frequency $0.9 f_0$	39
37. Difference Pattern, Amplitude and Phase Illumination; Scan Angle $\theta_0 = 1.2^\circ$ , Frequency $0.9 f_0$	40
38. Difference Pattern; Scan Angle $\theta_0 = 1.2^\circ$ , Frequency $0.9 f_0$	40
39. Difference Pattern, Amplitude and Phase Illumination; Scan Angle $\theta_0 = 2.4^\circ$ , Frequency $0.9 f_0$	41
40. Difference Pattern; Scan Angle $\theta_0 = 2.4^\circ$ , Frequency $0.9 f_0$	41
41. Sum Pattern, Amplitude and Phase Illumination; Scan Angle $\theta_0 = 3.6^\circ$ , Frequency $0.9 f_0$	42
42. Difference Pattern; Scan Angle $\theta_0 = 3.6^\circ$ , Frequency $0.9 f_0$	42
43. Amplitude and Phase Illumination of Subarray 1R, Frequency $1.1 f_0$	43
44. Radiation Pattern of Subarray 1R, Frequency $1.1 f_0$	43
45. Amplitude and Phase Illumination of Subarray 4R, Frequency $1.1 f_0$	44
46. Radiation Pattern of Subarray 4R, Frequency $1.1 f_0$	44
47. Sum Pattern, Amplitude and Phase Illumination; Scan Angle $\theta_0 = 0^\circ$ , Frequency $1.1 f_0$	45
48. Sum Pattern; Scan Angle $\theta_0 = 0^\circ$ , Frequency $1.1 f_0$	45
49. Sum Pattern, Amplitude and Phase Illumination; Scan Angle $\theta_0 = 0^\circ$ , Frequency $1.1 f_0$	46
50. Sum Pattern; Scan Angle $\theta_0 = 1.2^\circ$ , Frequency $1.1 f_0$	46
51. Sum Pattern, Amplitude and Phase Illumination; Scan Angle $\theta_0 = 2.4^\circ$ , Frequency $1.1 f_0$	47
52. Sum Pattern; Scan Angle $\theta_0 = 2.4^\circ$ , Frequency $1.1 f_0$	47
53. Sum Pattern, Amplitude and Phase Illumination; Scan Angle $\theta_0 = 3.6^\circ$ , Frequency $1.1 f_0$	48
54. Sum Pattern; Scan Angle $\theta_0 = 3.6^\circ$ , Frequency $1.1 f_0$	48
55. Difference Pattern, Amplitude and Phase Illumination; Scan Angle $\theta_0 = 0^\circ$ , Frequency $1.1 f_0$	49
56. Difference Pattern; Scan Angle $\theta_0 = 0^\circ$ , Frequency $1.1 f_0$	49

## Illustrations

57. Difference Pattern, Amplitude and Phase Illumination; Scan Angle $\theta_0 = 1.2^\circ$ , Frequency $1.1 f_0$	50
58. Difference Pattern; Scan Angle $\theta_0 = 1.2^\circ$ , Frequency $1.1 f_0$	50
59. Difference Pattern, Amplitude and Phase Illumination; Scan Angle $\theta_0 = 2.4^\circ$ , Frequency $1.1 f_0$	51
60. Difference Pattern; Scan Angle $\theta_0 = 2.4^\circ$ , Frequency $1.1 f_0$	51
61. Difference Pattern, Amplitude and Phase Illumination; Scan Angle $\theta_0 = 3.6^\circ$ , Frequency $1.1 f_0$	52
62. Difference Pattern; Scan Angle $\theta_0 = 3.6^\circ$ , Frequency $1.1 f_0$	52
63. Illumination Efficiency vs Scan Angle	53
64. Composite Hybrid Network	59

## Tables

1. Sum and Difference Illumination Coefficients	20
---	----

# Design Criteria and Numerical Simulation of an Antenna System for One-Dimensional Limited Scan

## 1. INTRODUCTION

In recent years, a number of studies have been devoted to limited scan antenna techniques.<sup>1</sup> The goal of these studies has been the reduction of the number of costly control elements (phase shifters or variable power dividers) as compared to the number in a phased array that is designed in a "conventional" way using a phase shifter for each elementary radiator. Actually, in the latter case, the antenna aperture is the main factor determining the number of elements. Narrowing the field of view (FOV) produces only a limited saving on the number of phase shifters over those used in a wide angle antenna system because the maximum element spacings are constrained in order to avoid grating lobes. Therefore, the antenna gain rather than the scan sector is the factor that mainly affects the number of phase shifters. A substantial reduction of the number of control elements in an antenna system for limited scan can be obtained only with totally different design schemes.

In several of the proposed solutions, a limited scan is achieved by using a small array located in the focal region of a microwave optical system whose magnifying effect is exploited in some way. The aperture is in most cases inefficiently used because for each scan direction, only a limited part of it is actually

(Received for publication 28 November 1975)

1. Mailloux, R. J., and Blacksmith, P. (1974) Array and reflector techniques for airport precision approach radars, Microwave J., pp 35-38.

radiating.<sup>2,3</sup> In the design scheme described in ref. 3 the design is optimized from the viewpoint of the minimization of the number of control elements.

The system proposed in this report is based on the idea of synthesizing the aperture illumination by using overlapping subarrays whose excitations are independently controlled. The concept was probably originated by A. Rudge,<sup>4</sup> and pursued by R. Tang.<sup>5</sup> Both these authors did not present a detailed analysis or design procedure. The contributions of this paper consist of providing detailed analysis and design criteria for a specific antenna configuration, for limited scan in one plane, having a number of very desirable features:

- The number of phase shifters is the theoretical minimum for the given aperture size and FOV.<sup>6</sup>
- The aperture is fully used with high efficiency.
- The beam pointing and width are approximately constant for a moderate change of frequency, so providing wide instantaneous bandwidth.
- Ultralow sidelobes outside the FOV can be obtained at the expense of a slight decrease of the illumination efficiency.
- The aperture illumination can be accurately controlled, yielding excellent sum and difference pattern specified independently.

The structure consists of a cylindrical lens with a linear outer aperture and a circular inner profile. The lens is a Rotman "bootlace" type. This means that corresponding collecting and radiating elements - at the inner and outer faces of the lens - equidistant from the lens axis are electrically connected through equal lengths of coaxial cables. A linear focused array is located on the focal plane, and fed by a hybrid network (with a number of radiation ports greater than the number of input ports). A beam forming network, providing separate control of sum and difference patterns, feeds the hybrid network through a set of phase shifters whose number is approximately equal to the product of aperture length (in wavelengths) by FOV (in " $\sin\theta$  space").

For a numerical investigation an antenna with a 3 dB beamwidth of  $1.2^\circ$  with a nominal scan sector of approximately 6 beamwidths has been considered. The numerical results of computer simulation-antenna patterns, lens aperture illuminations, and focal array illuminations confirm the theoretical expectation of excellent performance. The behavior on a 20 percent bandwidth centered around the design

2. Winter, C. (1968) Phase scanning experiments with two reflector antenna systems, Proc. IEEE 56(No. 11).
3. Schell, A. C. (1972) A Limited Sector Scanning Antenna, IEEE G-AP International Symposium.
4. Rudge, A. W., and Whithers, M. J. (1971) New techniques for beam steering with fixed parabolic reflectors, Proc. IEE (British) 118(No. 7):857-863.
5. Tang, R. (1972) Survey of Time-Delay Beam Steering Techniques, Proc. 1970 Phased Array Antenna Symp., Artech House, pp 254-260.
6. Borgiotti, G. V. (1975) Degrees of Freedom of an Antenna Scanned in a Limited Sector, IEEE G-AP International Symp, pp 319-320.

frequency is also investigated with the purpose of assessing the broadband properties of the system. It is shown that the main effect of frequency change is to vary the level of the far out sidelobes. Instead the main beam shape and pointing and the sidelobes inside the FOV are only slightly affected.

In the analysis, no mutual coupling effects on the lens elements were considered. This means that in the frequency band of interest, the various apertures are assumed matched. Because the scan sector is limited, this condition is not difficult to achieve. However, the discussion of this point is outside the scope of this report.

The report is organized as follows. In Section 2, the idea of synthesizing an array illumination by using translated interpolating functions (overlapping subarrays) is introduced. In Section 3, an antenna configuration practically implementing the concept is considered and an accurate mathematical model developed. The theory of operation is discussed in Section 4 by using a simplified analytical model. An outline of the design procedure for a particular case is presented in Section 5; in Section 6 the calculated performances are discussed. In Appendix A, a special hybrid network scheme is considered, and in Appendix B an approximate analysis of phase quantization effects is developed.

## 2. THE OVERLAPPING SUBARRAY CONCEPT

In this section we will discuss in detail the overlapping subarray concept in order to establish several relationships which form the foundation of the proposed antenna system design. The antenna configuration and its theory of operation are described in Sections 3 and 4.

Let  $2a$  be the aperture length and  $x$  an abscissa on it. Let  $u$ ,

$$u = \frac{2\pi}{\lambda} \sin\theta, \quad (1)$$

be an abscissa on the wavenumber axis, where  $\theta$  is the angle from broadside direction and  $\lambda$  is the wavelength of operation. If the polarization is in the plane of incidence, the relationship between the radiation pattern  $g(u)$  and the antenna illumination  $f(x)$  is given by the Fourier transformation:

$$g(u) = \int_{-a}^a f(x) \exp(jux) dx. \quad (2)$$

Let  $2\alpha$  be the actual angular width of the FOV greater than the nominal scan sector to take into account the beamwidth of the radiated beam (as discussed later).

Put

$$u_\epsilon = \frac{2\pi}{\lambda} \sin \epsilon \quad (3)$$

With the usual notation put:

$$\text{rect} \frac{u}{2u_\epsilon} = \begin{cases} 1 & \text{for } |u| \leq u_\epsilon \\ 0 & \text{for } |u| > u_\epsilon \end{cases} \quad (4)$$

Let us consider a function  $g_0(u)$  different from zero only in the FOV which, of course, is unrealizable as a radiation pattern generated by a finite aperture. A representation of  $g_0(u)$  is the following:

$$g_0(u) = \text{rect} \frac{u}{2u_\epsilon} \sum_p a_p \exp\left(jp \pi \frac{u}{u_\epsilon}\right) \quad (5)$$

$$\left(p = \dots, -\frac{3}{2}, -\frac{1}{2}, \frac{1}{2}, \frac{3}{2}, \dots\right).$$

Equation (5) is recognized to be a conventional Fourier series of period  $2u_\epsilon$  multiplied by a linear phase term. It is easy to show that the terms of Eq. (5) form a complete system of functions in  $-u_\epsilon, u_\epsilon$ . Thus Eq. (5) can be used instead of a more conventional Fourier series (that is, one with the indexes  $p$  taking integer values). The reason for choosing this expansion will be apparent in the sequel. It is related to the use of a hybrid network with an even number of input ports. By taking the inverse F. T. of Eq. (5) and then truncating it to the length  $2a$  of the aperture, one obtains the aperture illumination  $f(x)$  that provides the best rms realizable approximation on the entire  $u$  axis of the unrealizable pattern of Eq. (5):

$$f(x) = \text{rect} \frac{x}{2a} \sum_p a_p \frac{\sin u_\epsilon \left(x - p \frac{\pi}{u_\epsilon}\right)}{u_\epsilon \left(x - p \frac{\pi}{u_\epsilon}\right)} \quad (6)$$

where constant factors have been neglected.

Equation (6) represents the antenna illumination as a weighted sum of "overlapping subarrays" whose centers lie in the equispaced points:

$$x_p = p \frac{\pi}{u_\epsilon} = p \frac{\lambda}{2 \sin \epsilon} \quad \left(p = \dots, -\frac{3}{2}, -\frac{1}{2}, \frac{1}{2}, \frac{3}{2}, \dots\right) \quad (7)$$

Because of their oscillating behavior, the contributions to the radiation pattern inside the FOV, of the terms of Eq. (6) for which  $x_p$  lies outside the aperture, are small. Thus the radiation pattern will not change substantially if the sum of

Eq. (6) is truncated by retaining only those terms for which the subarray centers belong to the aperture. Thus we will write for the illumination with self-explanatory notation:

$$f(x) = \text{rect} \frac{x}{2a} \sum_{|x_p| < a} a_p \frac{\sin \left[ u_\epsilon \left( x - p \frac{\pi}{u_\epsilon} \right) \right]}{u_\epsilon \left( x - p \frac{\pi}{u_\epsilon} \right)}. \quad (8)$$

The radiation pattern of a single subarray is given by the convolution (neglecting multiplicative constants):

$$g_p(u) = \frac{\sin au}{u} \otimes \left[ \text{rect} \frac{u}{2u_\epsilon} \exp \left( jp \frac{\pi}{u_\epsilon} u \right) \right], \quad (9)$$

and thus is given by a rectangular waveform multiplied by a linear phase term "filtered" by the pattern of the uniformly illuminated aperture. Terms with higher  $|p|$ 's correspond to subarray illuminations centered in points closer to the aperture edges, and are therefore more severely truncated by the aperture finite length. Their patterns thus deviate more and more from a rectangular shape, as is numerically shown in Section 6.

The choice of the coefficients  $a_p$  is made simply by sampling a desirable illumination for a continuous aperture in the points of Eq. (7). In this way we obtain for the pattern a periodic function filtered out by the subarray patterns which limit the radiation essentially to the FOV. The procedure, considering a numerical example, will be discussed in Section 5.

We proceed now to the discussion of a design scheme for the practical implementation of the concepts outlined above.

### 3. ANTENNA CONFIGURATION AND ANALYTICAL MODEL

With reference to Figure 1, consider a "bootlace" cylindrical plane-circular lens. Corresponding collecting and radiating elements on the two faces (located at the same distance  $x$  from the lens axis) are connected through equal cable lengths.

Denote the focal length, equal also to the radius of the inner lens profile by  $F$ . Recalling that  $2a$  is the aperture length, let

$$\sin \theta_a = \frac{a}{F}, \quad (10)$$

where  $\theta_a$  is the lens half angular aperture. With the notation of the preceding section, denote the ratio ("magnification") by  $\mu$ :



$$\phi(\xi) = \frac{2\pi}{\lambda} \sqrt{\xi^2 + F^2} . \quad (13)$$

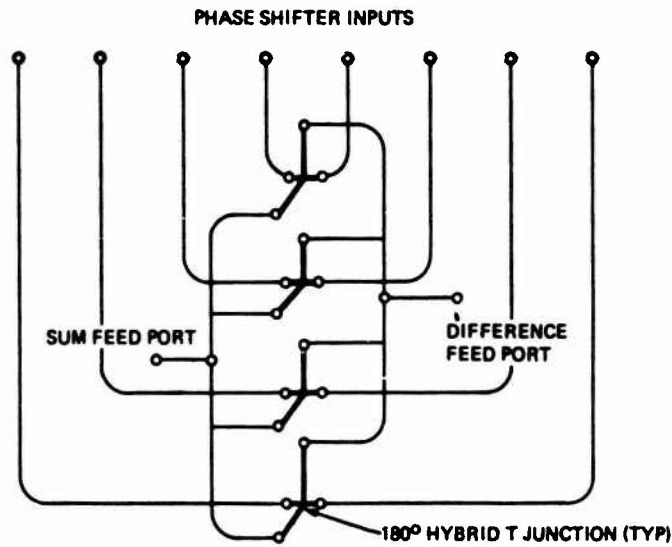


Figure 2. Beam Forming Network for Independent Control of Sum and Difference Patterns

Assume that the number of input ("equipment") ports of the hybrid network is even and equal to  $N$ . When only one of the ports, denoted by the subscript  $p$ , is excited by a unitary incident wave, the excitation of an element whose center is located at the abscissa  $\xi$ , is

$$m_p(\xi) = \text{rect} \frac{\xi}{2b} \exp\left(-j \frac{\pi}{b} p \xi\right) \exp\left[j\phi(\xi)\right] \\ \left(p = -\frac{N-1}{2}, -\frac{N-1}{2} + 1, \dots, \frac{N-1}{2}\right) \quad (14)$$

where the phase transformation of Eq. (13) has been included.

Let us consider how the sum pattern is generated. Parallel discussion applies to the difference pattern. When the sum port of the BFN is excited, the  $N$  outputs will be a set of equiphase voltages  $\{a_{\Sigma}(p)\}$ , whose magnitudes are chosen to be equal to the samples of "good" illumination at the locations of the subarray centers. Suppose now that the phase shifters are set to introduce phase delays  $\phi_p$  proportional to the abscissae of the subarray centers on the lens aperture. Then

$$\phi_p = \frac{2\pi}{\lambda} x_p \sin\theta_0 \quad (15)$$

where the  $x_p$ 's are given by Eq. (7). We shall see, when discussing the theory of operation in Section 4, that  $\sin\theta_0$  is the sine of the scan direction. Because of Eq. (7), the abscissa  $x_p$  is proportional to  $\lambda$ . Thus the phase settings of Eq. (15) are independent of frequency, and can be written as

$$\phi_p = -p\pi \frac{\sin\theta_0}{\sin\epsilon} \quad (16)$$

with  $p$  taking half integer values. Since the focal array elements have been assumed as being closely spaced ( $\sim\lambda/2$ ), the actual array aperture distribution generated by discrete elements can be replaced in our analysis by a continuous distribution obtained by assuming that in Eq. (14)  $\xi$  takes continuous values. Thus by using superposition, we obtain for the sum illumination of the focal array [see Eq. (14)]

$$I_\Sigma(\xi|\theta_0) = \text{rect} \frac{\xi}{2b} \sum_{p=-\frac{N-1}{2}}^{\frac{N-1}{2}} a_\Sigma(p) m_p(\xi) \exp\left(-jp\pi \frac{\sin\theta_0}{\sin\epsilon}\right) \quad (17)$$

(Replacing the subscript  $\Sigma$  with  $\Delta$ , one obtains the expression for the difference illumination on the focal array.) The antenna aperture illumination (on the outer lens face) is therefore found to be (neglecting constants)

$$f_\Sigma(x|\theta_0) = \text{ret} \frac{x}{2b} \cdot \int_{-b}^b \left(F^2 + \xi^2 - 2x\xi\right)^{-1/4} I_\Sigma(\xi|\theta_0) \exp\left[j \frac{2\pi}{\lambda} \left(F^2 + \xi^2\right)^{1/2} - j \frac{2\pi}{\lambda} \left(F^2 + \xi^2 - 2x\xi\right)^{1/2}\right] d\xi \quad (18)$$

According to Eq. (2), the antenna pattern is

$$g_\Sigma(u|\theta_0) = \int_{-a}^a f_\Sigma(x|\theta_0) \exp(jux) dx \quad (19)$$

Expressions parallel to Eqs. (18) and (19) hold for the difference illumination and pattern.

#### 4. THEORY OF OPERATION

The various relationships established in the preceding section provide an accurate analytical model of the system and have been used for the computer simulation of the antenna performance. However, to gain an insight into the way the antenna system works, it is convenient to resort to a simplified theory that more clearly illustrates certain basic features of the design scheme.

Consider Eq. (18). The amplitude term can be expanded with respect to  $\xi/F$  as follows:

$$\left(F^2 + \xi^2 - 2x\xi\right)^{-1/4} = F^{-1/2} \left(1 + \frac{x\xi}{F^2} + \text{higher order terms}\right). \quad (20)$$

The maximum absolute value that the first order term in square brackets can take is [see Eqs. (11) and (12)]

$$\frac{1}{2} \sin \theta_a \sin \epsilon \ll 1. \quad (21)$$

Thus we may replace the amplitude term in Eq. (17) with a constant. With regard to the phase term, by again expanding with respect to  $\xi/F$  we can write

$$- \frac{2\pi}{\lambda} \left[ \sqrt{F^2 + \xi^2 - 2x\xi} - \sqrt{F^2 + \xi^2} \right] = \frac{2\pi}{\lambda} \left[ \frac{x\xi}{F} - \frac{(x\xi)^2}{2F^3} + \text{higher order terms} \right]. \quad (22)$$

Neglecting terms of order higher than the first in Eq. (22) has a negligible effect on the integral of Eq. (18) provided that their phase contribution at the aperture edge (where it is maximum) is small. We postulate that only the first order term in the series of Eq. (22) should be retained if for every  $x$  and  $\xi$  the second order term is less than a radian. This leads to the condition

$$\pi \left(\frac{F}{\lambda}\right) (\sin \theta_a)^2 (\sin \epsilon)^2 < 1. \quad (23)$$

Assuming that Eq. (23) holds (as discussed for the numerical example in Section 5), we can write for Eq. (18), neglecting unessential multiplicative constants,

$$f_{\Sigma}(x|\theta_0) \approx \sum_{p=-\frac{N-1}{2}}^{\frac{N-1}{2}} a_{\Sigma}(p) \exp\left(-jp\pi \frac{\sin \theta_0}{\sin \epsilon}\right) \cdot \left\{ \text{rect} \frac{x}{2a} \int_{-b}^b \exp\left[j\xi \left(\frac{2\pi}{\lambda F} x - p \frac{\pi}{b}\right)\right] d\xi \right\}. \quad (24)$$

Consider the integrals in Eq. (24). By recalling that

$$b = F \sin \epsilon$$

and referring to Eq. (3), one obtains

$$\int_{-b}^b \exp \left[ j \xi \left( \frac{2\pi}{\lambda F} x - p \frac{\pi}{b} \right) \right] d\xi = \frac{2 \sin \left[ u_{\epsilon} \left( x - \frac{p\pi}{u_{\epsilon}} \right) \right]}{\frac{2\pi}{\lambda F} \left( x - \frac{p\pi}{u_{\epsilon}} \right)}, \quad (25)$$

which, a constant apart, is the subarray illumination desired [see Eqs. (7) and (8)]. Inserting Eq. (25) into Eq. (24), we find that the illumination takes the form of Eq. (8) that is sought. The corresponding radiation pattern is, paralleling Eq. (9)

$$g_{\Sigma}(u | \theta_0) = \frac{\sin au}{u} \otimes \left[ \text{rect} \frac{u}{2u_{\epsilon}} \mid \sum_{|x_p| < a} a_{\Sigma}(p) \exp \left( jp\pi \frac{u-u_0}{u_{\epsilon}} \right) \right]. \quad (26)$$

Equation (26) expresses the radiation pattern as the convolution of a term, in square brackets, that has the meaning of an array factor (a periodic function) multiplied by a rectangular "element factor", and a term that represents the effect of the truncation of the subarrays due to the finite aperture size  $2a$ . Thus, the term in square brackets represents a non-realizable pattern strictly limited to the FOV. The convolution with the aperture function [the first term in Eq. (26)] expresses the physical realizability of the pattern with the given aperture. The pattern has its peak at  $u_0$  for the set of coefficients  $a_{\Sigma}(p)$  real and positive. Thus the phase settings of Eq. (16) are those to be given to obtain the scan in the wanted direction. Notice that for the sum pattern, the illumination coefficients are even with respect to  $p$ ;

$$a_{\Sigma}(p) = a_{\Sigma}(-p), \quad (27)$$

while the coefficients of the difference pattern will have an odd symmetry

$$a_{\Delta}(p) = -a_{\Delta}(-p). \quad (28)$$

It is thus recognized that the difference pattern has a zero in the direction  $\theta_0$  if the phase shifter settings at the input of the hybrid matrix are given by Eq. (16).

Several interesting features of Eq. (26) [and of its companion for the difference pattern] become apparent if, in the term in square brackets, the variable  $u$  is written as a function of  $\theta$  and  $\lambda$ :

$$\begin{aligned} \text{rect} \frac{u}{2u_\epsilon} \sum_{|x_p| < a} a_{\Sigma}(p) \exp\left(-j \frac{u-u_0}{u_\epsilon}\right) &= \\ = \text{rect} \frac{\sin\theta}{2 \sin\epsilon} \sum_{|x_p| < a} a_{\Sigma}(p) \exp\left(-j \frac{\sin\theta - \sin\theta_0}{\sin\epsilon}\right). & \quad (29) \end{aligned}$$

First notice that the angular extension of the subarray pattern of rectangular shape—in absence of aperture truncation—is independent of frequency. The physical reason becomes clear by recalling the way the subarrays are generated. By increasing the frequency, the focused beams radiated by the focal arrays for each input port excitation of the hybrid matrix become more concentrated, as do the subarray illuminations on the secondary lens aperture. The subarray radiation patterns should therefore increase their widths. However, this effect is compensated for exactly by the beamwidth narrowing due to frequency increase. Also, the correct subarray spacings are preserved with change in frequency. Notice however that the compensation is exact only for the linear-circular geometry of the lens profiles here considered. Notice also that the array factor in Eq. (29), directly related to beamwidth, is a function of  $\sin\theta$ , independent of frequency.

Another point is also interesting from a practical viewpoint. If the phase shifters have insertion phases approximately independent of frequency (in a limited band of interest) and if the hybrid network provides, for each input port excitation, a phase slope independent of frequency, then the settings of Eq. (16) of phase shifters for steering the beam in  $\theta_0$  direction are independent of frequency. In other words, the beam does not experience a "natural" scan due to a frequency variation. The physical reason is that when the frequency changes, the variation of spacing between subarray peaks produces in turn the exact phase slope change on the secondary aperture necessary to keep the beam direction fixed. Again this compensation is exact only for the particular lens-array geometry here discussed.

Considering Eq. (29) instead of Eq. (26) amounts to neglecting the subarray truncations due to the finite aperture of the lens. The results discussed above, however, still hold with excellent approximation when taking into account such an effect, which amounts to having the subarray patterns spreading somewhat outside the FOV. The question will be considered in detail in Section 6 when discussing the calculated performance of a particular antenna configuration.

## 5. DESIGN PROCEDURE AND COMPUTER SIMULATION OF A PARTICULAR CASE

We will now discuss the computer simulation of a particular case. In doing this, we will also briefly outline the step-by-step design procedure of the antenna system.

Assume that the specified half power beamwidth of the sum pattern is

$$\theta_{3\text{dB}} \approx 1.2^\circ \quad (30)$$

with first (and highest) sidelobe not higher than -25 dB. The aperture illumination to be approximated by overlapping subarrays is chosen for the sum pattern to be a Taylor distribution with  $\bar{n} = 5$  and sidelobe level -25 dB.<sup>8</sup> Consequently the aperture length is chosen to be

$$2a = 50\lambda_0 \quad (31)$$

where  $\lambda_0$  is the wavelength at center frequency. This yields for the theoretical 3 dB beamwidth a value equal to  $1.207^\circ$ , close enough to that specified in Eq. (30). From the discussion of Section 4 it follows that in order to make the behavior of the system close to the theoretical one, it is convenient to choose a long focal design. Thus we will assume, as shown in Figure 1, that

$$\frac{a}{F} = \sin\theta_a = 0.5, \quad \theta_a = 30^\circ. \quad (32)$$

The extent of the limited scan sector is assumed to be specified equal to  $8^\circ$ . However, the FOV  $2\epsilon$  is taken approximately a beamwidth wider; in this way, at the edge of the scan sector, most of the main sum beam will be inside the FOV and its periodic replicas outside it.

At center frequency  $f_0$  we will require that the edges of the aperture will coincide approximately with the outer 3 dB points of the main lobes of the subarray illuminations closest to the aperture edges. The number of subarrays  $N$  is given by the ratio between aperture length and subarray spacing. Thus, from Eq. (7)

$$N = \frac{2a}{\lambda} 2 \sin\epsilon \quad (33)$$

with  $N$  an integer number.  $N$  has the form of a product, aperture (in wavelengths) by FOV (in  $\sin\theta$ ), and is equal to the minimum theoretical number of control elements necessary to steer the beam in the FOV.<sup>6</sup>

8. Taylor, T. T. (1955) Design of line source antennas for narrow beamwidth and low sidelobes, IRE Tran. AP-3:16-28.

Since  $2\epsilon$  should be close to  $9.2^\circ$ , Eq. (33) gives, with the actual aperture size

$$N = 8; \quad \sin\epsilon = 0.08 \text{ (that is, } \epsilon = 4.58^\circ \text{)}.$$

The magnification factor is

$$\mu = \frac{\sin\theta_a}{\sin\epsilon} = 6.25, \quad (34)$$

and the focal array size is

$$2b = \frac{2a}{\mu} = 8\lambda_0. \quad (35)$$

The number of radiating elements of the focal array is chosen equal to 16, thus their size is half wavelength at center frequency. The elements are fed by a hybrid network with 8 inputs and 16 outputs, and each output is time delayed according to Eq. (13) [which represents a time advance since we have dropped terms independent of  $\xi$ ]. The hybrid network can be either a 16 by 16 matrix, whose only inputs corresponding to the 8 beams closer to broadside are excited, or any other structure whose input-output behavior is equivalent to it (see Appendix A). Thus the array illumination, when the port  $p$  is excited, is given by Eq. (14) where  $p$  can take the values

$$p = -\frac{7}{2}, -\frac{5}{2}, -\frac{3}{2}, -\frac{1}{2}, \frac{1}{2}, \frac{3}{2}, \frac{5}{2}, \frac{7}{2}. \quad (36)$$

The hybrid network is fed through a set of phase shifters by a BFN providing a separate control of the sum and difference excitation (see Figure 2). The coefficients  $a_\Sigma(p)$  of the sum beam are obtained by sampling the Taylor distribution already mentioned ( $\bar{n} = 5$ , sidelobe level -25 dB) at the abscissae of the peaks of the subarrays (at center frequency). The odd illumination sampled in the same points to provide the coefficients  $a_\Delta(p)$  for the difference beam is the first anti-symmetric prolate spheroidal function with  $c = 8$ . The discussion of those choices for the illuminations is outside the scope of this report. The coefficients generated by the BFN are indicated in Table 1. Notice that in our case

$$\pi \frac{F}{\lambda} (\sin\theta_a)^2 (\sin\epsilon)^2 = 0.251,$$

$$\frac{1}{2} \sin\theta_a \sin\epsilon = 0.02.$$

Table 1. Sum and Difference Illumination Coefficients  $\left[ a_{\Sigma}(-p) = a_{\Sigma}(p) \quad a_{\Delta}(-p) = -a_{\Delta}(p) \right]$

p	a	$a_{\Delta}$
1/2	1	1
3/2	0.8508	-2.4400
5/2	0.5943	-2.4800
7/2	0.4249	-1.1200

Hence, on the basis of the discussion in Section 4, [see Eq. (21) and Eq. (23)], we expect the structure to behave in a way close to that analytically described in Section 2, with excellent performance. This is the case as shown by the numerical results discussed in the next section.

## 6. NUMERICAL RESULTS AND DISCUSSION

Extensive numerical analysis of the structure described in Section 5 has been made. Subarray illuminations and patterns, and sum and difference illuminations and patterns for various scan conditions have been evaluated by using the formulas developed in Section 3. To check the broadband properties discussed in Section 4, the calculations have been performed at three different frequencies:  $f_0$  (for which the aperture is 50 wavelengths long),  $0.9 f_0$ , and  $1.1 f_0$ . All the graphs have been computer generated. In some cases this fact is apparent by inspection of the plots showing the linear interpolation between computed points. The linear scale of ordinates for the amplitude illumination is arbitrary. The ordinates of the phase illumination are scaled in units of  $\pi$ , that is, one unit corresponds to a phase difference of  $180^\circ$ . The scale of abscissae for the illumination is normalized to unity at the aperture edges. Notice that the scale of abscissae for the radiation patterns is given in units of  $\sin\theta$ . When calculating sum and difference patterns, the phase shifter settings are those in Eq. (16) and thus for a given nominal steering angle  $\theta_0$  are the same for every frequency.

Figure 3 shows the amplitude and phase of the aperture illumination for center frequency  $f_0$  when one of the two ports of the hybrid network which generates a subarray located closest to the antenna axis is excited (the BFN assumed thus disconnected, see Figure 1). For this subarray and the one symmetric with respect to the antenna axis, the truncation due to finite aperture size is the least severe. Thus the pattern shape, Figure 4, is the closest to the ideal, "rectangular" form. Figure 5 shows the amplitude and phase illumination for excitation of port 4R of the hybrid network. The amplitude and phase plots are still those

expected, but the severe truncation generates a subarray pattern which has a relatively high level of radiated energy outside the FOV, and so is less similar to the ideal one (Figure 6). In Figures 7-14 the illuminations (amplitudes and phases) and the radiation patterns for the sum pattern for different directions of scan are shown. As described in previous sections, the illumination is obtained by weighting the subarray excitations (through the power divider constituting the BFN) with coefficients given in Table 1. Interestingly, during scan the amplitude illumination changes its shape substantially as Figures 7, 9, 11, and 13 show; the phase being almost exactly linear. The pattern within the FOV is close to the one theoretically expected, with a level of sidelobes of approximately -24 dB, and decaying rapidly outside. For scan angle of  $\theta_0 = 3.6^\circ$ , a grating lobe begins to appear, since the periodic replica of the main beam (at a distance  $2 \sin \theta$  on the  $\sin \theta$  axis) starts entering into the FOV. Figures 15-22 show phase and amplitude illuminations and radiation patterns for difference beams, still at frequency  $f_0$ . The illumination coefficients are given in Table 1. In this case, the pattern deteriorates substantially for a scan angle equal to  $3.6^\circ$  (Figure 22). This is, of course, expected since the periodic replica of the difference beam enters into the FOV for a scan angle less than that in the case of the sum beam (because the difference beam has a greater angular extension). Notice, however, that the null of the difference pattern still is in its nominal position. This suggests that in the absence of interference the pattern of Figure 22 is possibly still usable.

Figures 23-42 depict similar results for the frequency  $0.9 f_0$ . It is interesting that the 3 dB width of the pattern of the subarray 1R in Figure 24 is not significantly changed with respect to the corresponding one at frequency  $f_0$  (Figure 4). For the subarray 4R, because of the more severe truncation at the lower frequency (Figure 25), the decay of the pattern outside the FOV is slower than at  $f_0$  (Figure 26). The sum patterns of Figures 28, 30, 32, and 34 show higher sidelobes than those at the center frequency. However the direction of the peak of the beam does not change with frequency. Moreover the 3 dB beamwidth remains essentially the same. This point has been discussed in Section 4 where the array factor was shown to be approximately independent of frequency and can now be explained from a different viewpoint by comparing the amplitude illuminations at the frequency  $0.9 f_0$  with those at the frequency  $f_0$ . The illumination taper is much less for the lower frequency cases and this effect compensates the natural beam broadening due to frequency change. Similar remarks can be made for the difference patterns.

The last group of figures refers to the frequency  $1.1 f_0$ . In Figures 43 and 44 the amplitude and phase illuminations and the radiation pattern of the subarray 1R are plotted. The less severe truncation now leads to a faster sidelobe decay.

The same can be said for subarray 4R (Figures 45 and 46). Because of the more effective filtering effects due to the subarray patterns, the level of sidelobe level in the sum pattern drops immediately below -40 dB outside the FOV, as Figures 47-54 show, while being under -25 dB within it for all scan conditions. Similar remarks can again be made for the difference patterns. Again the variation of the sum 3 dB beamwidth with frequency is not easily detectable on the computer plots. Also, comparisons with the patterns at  $f_0$  show that the peak and null directions, for the phase settings [Eq. (16)], do not depend upon frequency, under our hypothesis of ideal phase shifters and hybrid network.

It is finally interesting to evaluate the efficiency of the illuminations, particularly for the case of frequency equal to  $1.1 f_0$  for which ultrasidelobes outside the FOV are obtained. The plots as function of scan angle are given in Figure 63, and show that the efficiency of the illumination is very high. Also, for the frequency  $1.1 f_0$  the slight decrease of efficiency is expected to be compensated by a smaller spillover loss (not calculated).

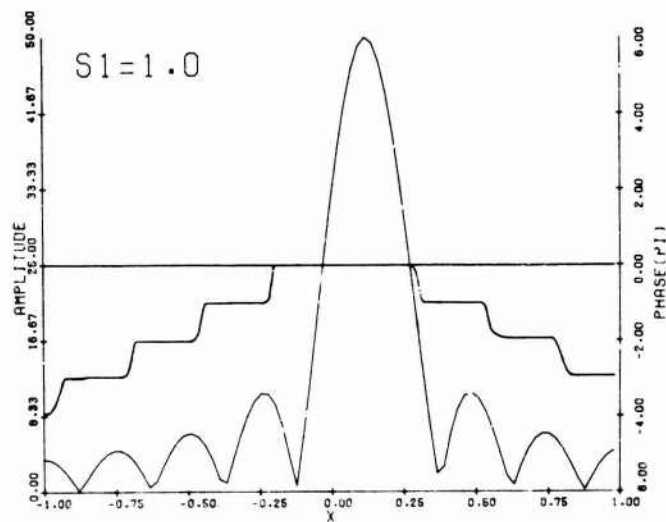


Figure 3. Amplitude and Phase Illumination of Subarray 1R, Frequency  $f_0$

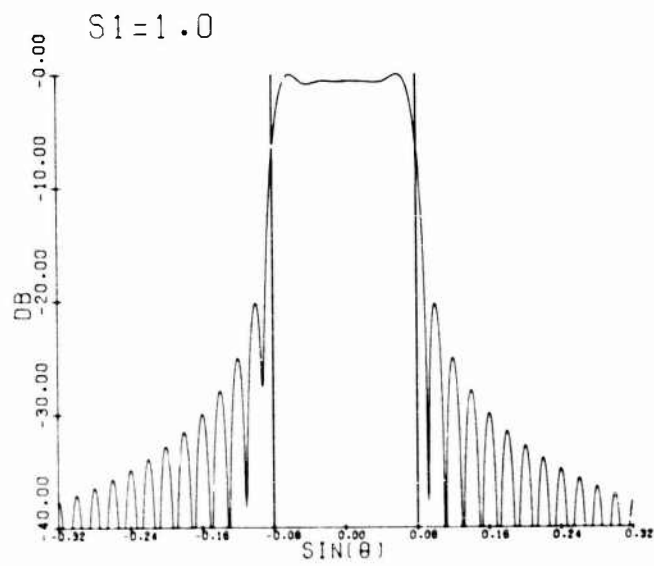


Figure 4. Radiation Pattern of Subarray 1R, Frequency  $f_0$

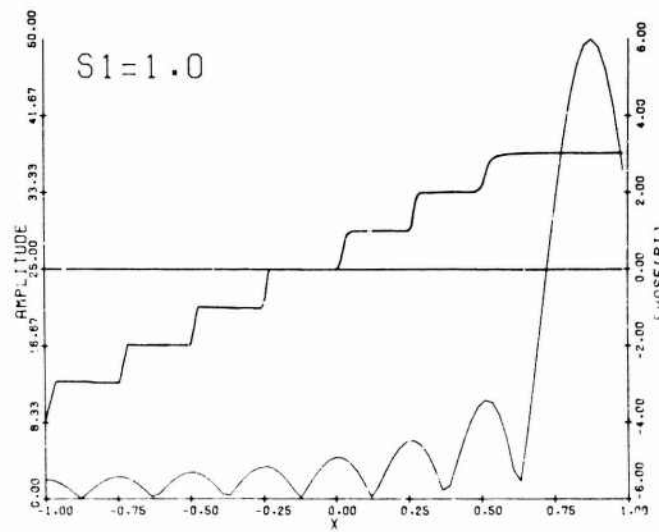


Figure 5. Amplitude and Phase Illumination of Subarray 4R, Frequency  $f_0$

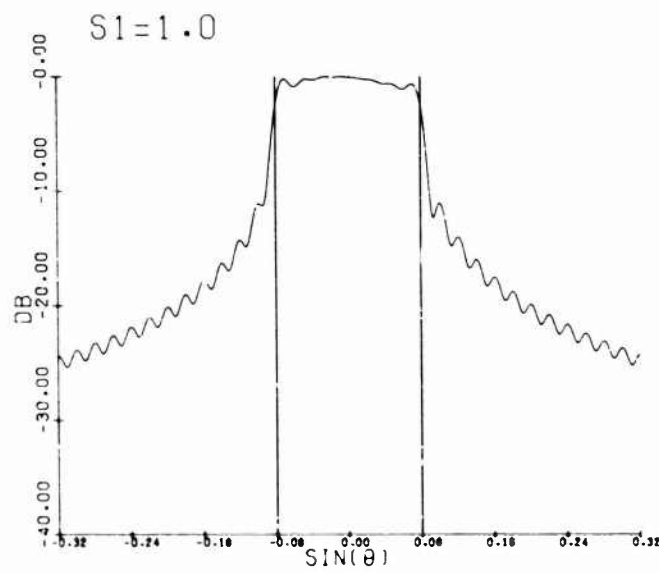


Figure 6. Radiation Pattern of Subarray 4R, Frequency  $f_0$

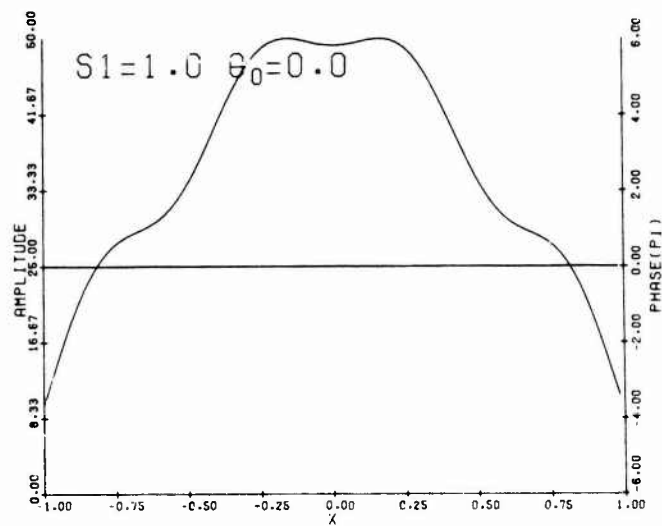


Figure 7. Sum Pattern, Amplitude and Phase Illumination; Scan Angle  $\theta_0 = 0^\circ$ , Frequency  $f_0$

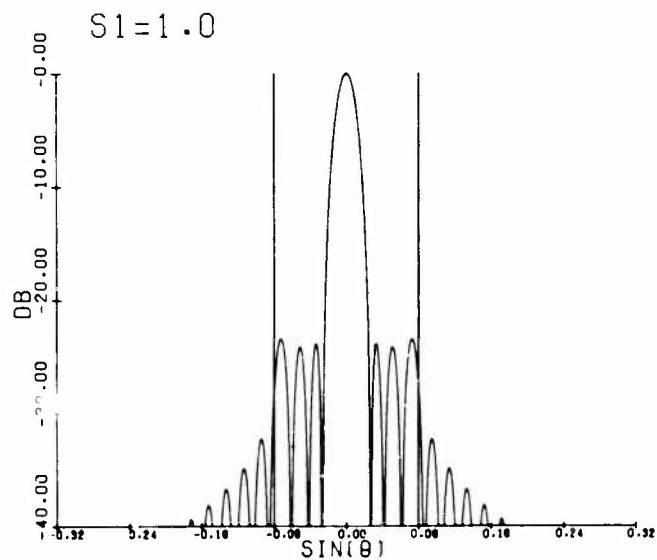


Figure 8. Sum Pattern; Scan Angle  $\theta_0 = 0^\circ$ , Frequency  $f_0$

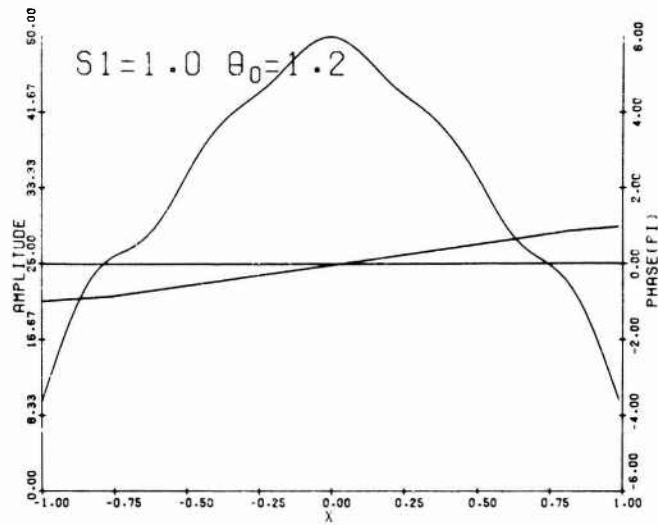


Figure 9. Sum Pattern, Amplitude and Phase Illumination; Scan Angle  $\theta_0 = 1.2^\circ$ , Frequency  $f_0$

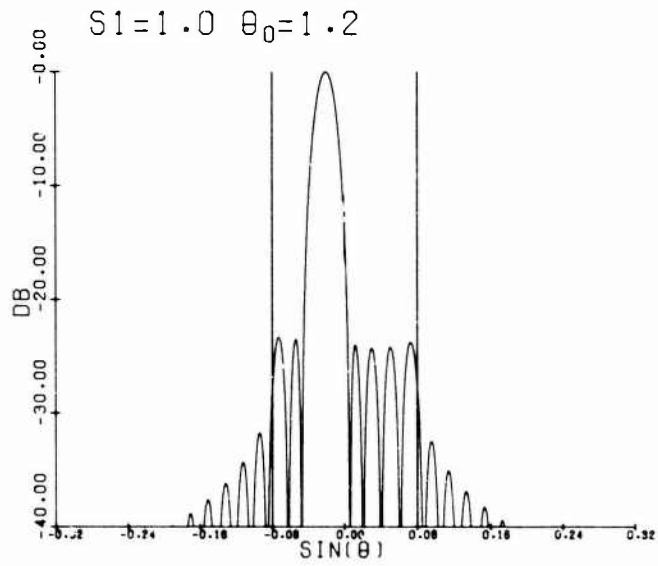


Figure 10. Sum Pattern; Scan Angle  $\theta_0 = 1.2^\circ$ , Frequency  $f_0$

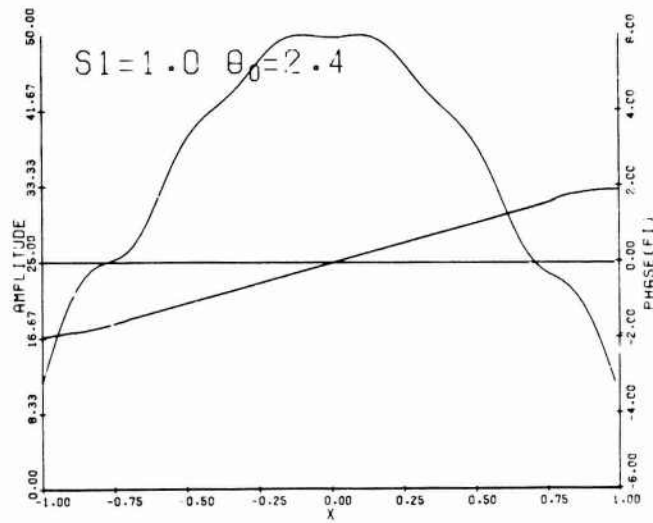


Figure 11. Sum Pattern, Amplitude and Phase Illustration; Scan Angle  $\theta_0 = 2.4^\circ$ , Frequency  $f_0$

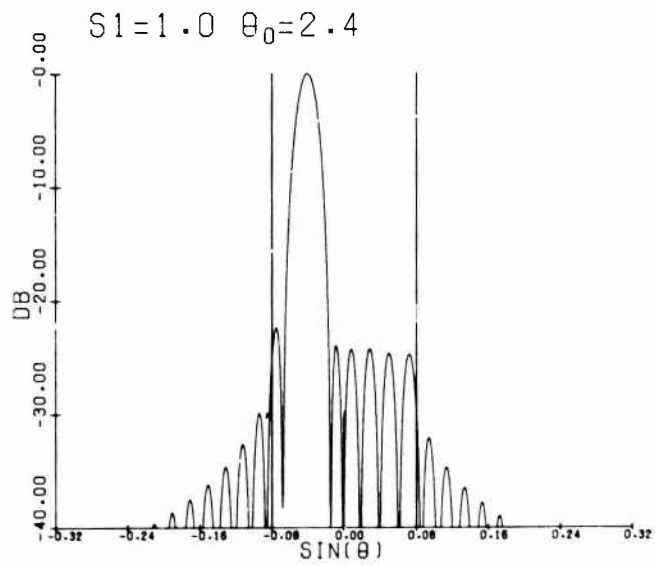


Figure 12. Sum Pattern; Scan Angle  $\theta_0 = 2.4^\circ$ , Frequency  $f_0$

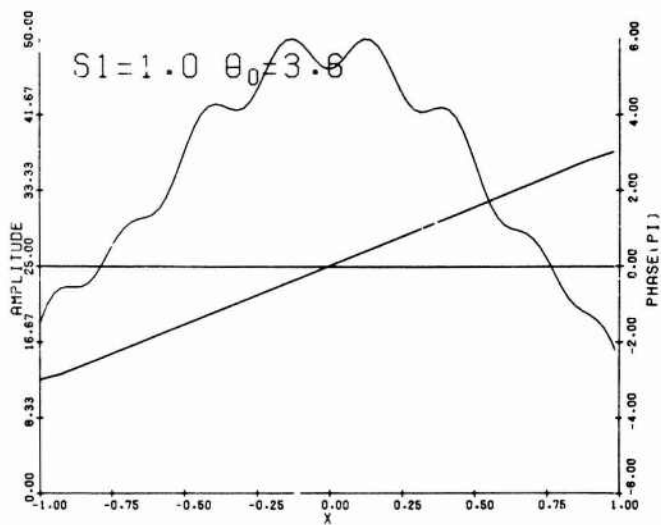


Figure 13. Sum Pattern, Amplitude and Phase Illumination; Scan Angle  $\theta_0 = 3.6^\circ$ , Frequency  $f_0$

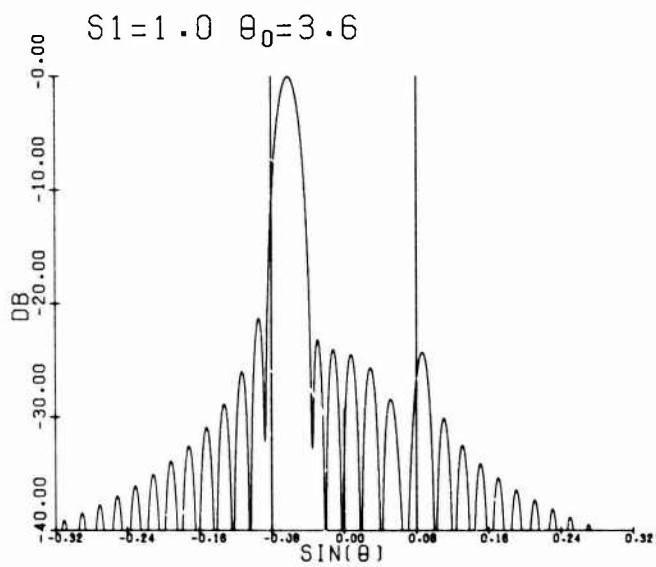


Figure 14. Sum Pattern; Scan Angle  $\theta_0 = 3.6^\circ$ , Frequency  $f_0$

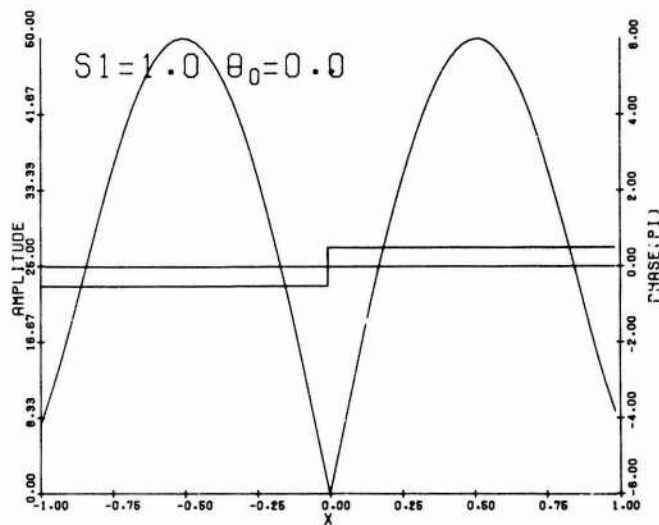


Figure 15. Difference Pattern, Amplitude and Phase Illumination; Scan Angle  $\theta_0 = 0^\circ$ , Frequency  $f_0$

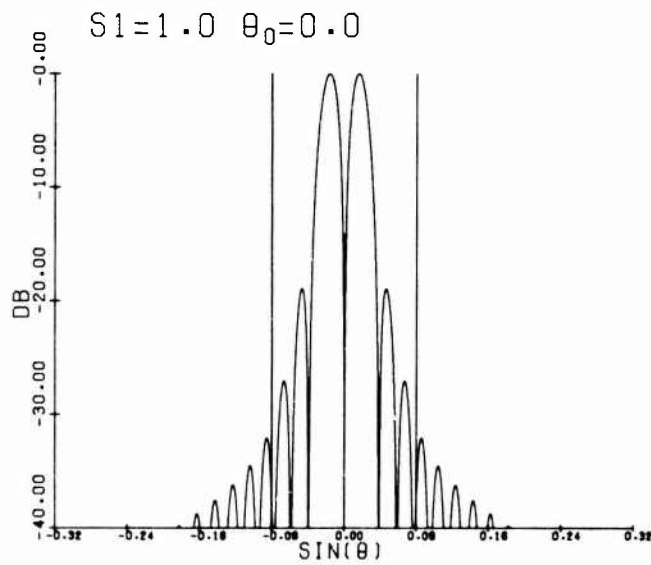


Figure 16. Difference Pattern; Scan Angle  $\theta_0 = 0^\circ$ , Frequency  $f_0$

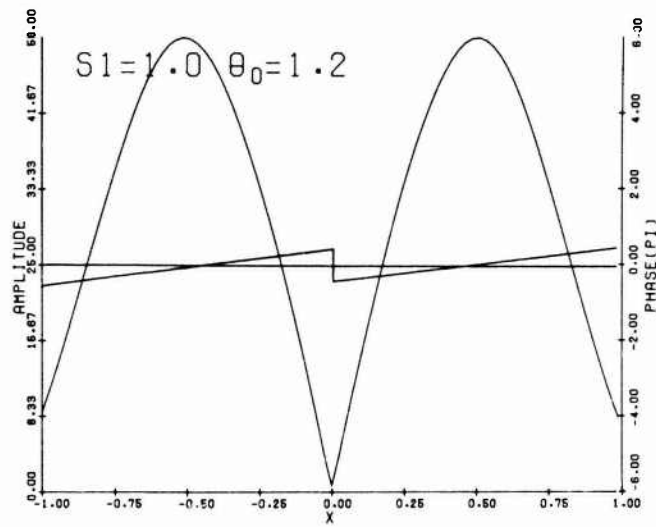


Figure 17. Difference Pattern, Amplitude and Phase Illumination; Scan Angle  $\theta_0 = 1.2^\circ$ , Frequency  $f_0$

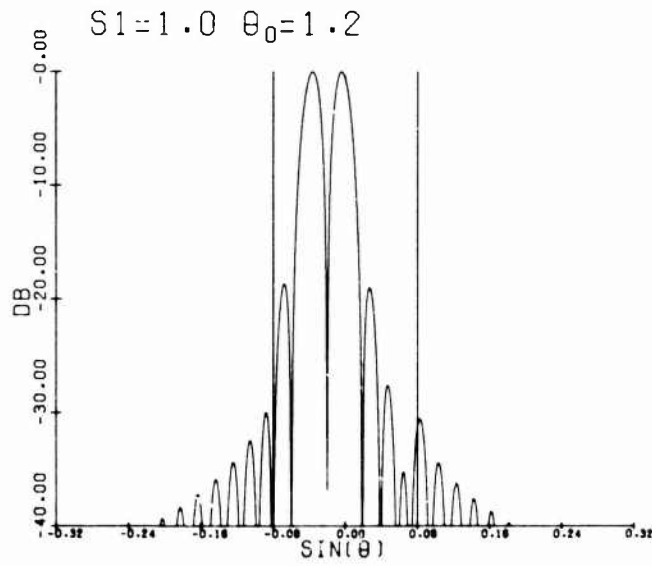


Figure 18. Difference Pattern; Scan Angle  $\theta_0 = 1.2^\circ$ , Frequency  $f_0$

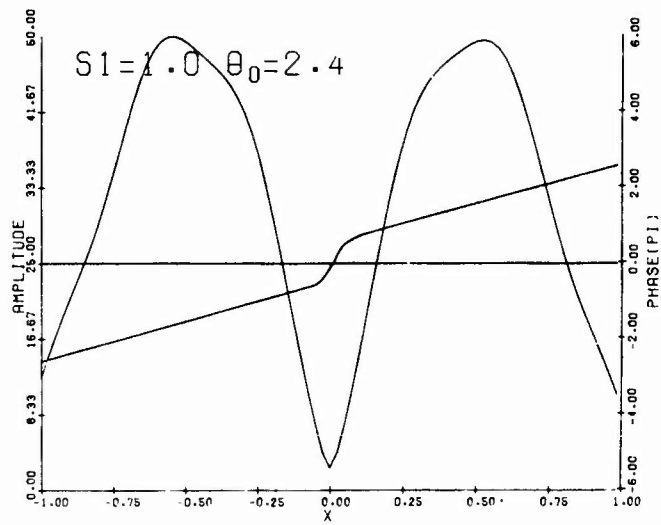


Figure 19. Difference Pattern, Amplitude and Phase Illumination; Scan Angle  $\theta_0 = 2.4^\circ$ , Frequency  $f_0$

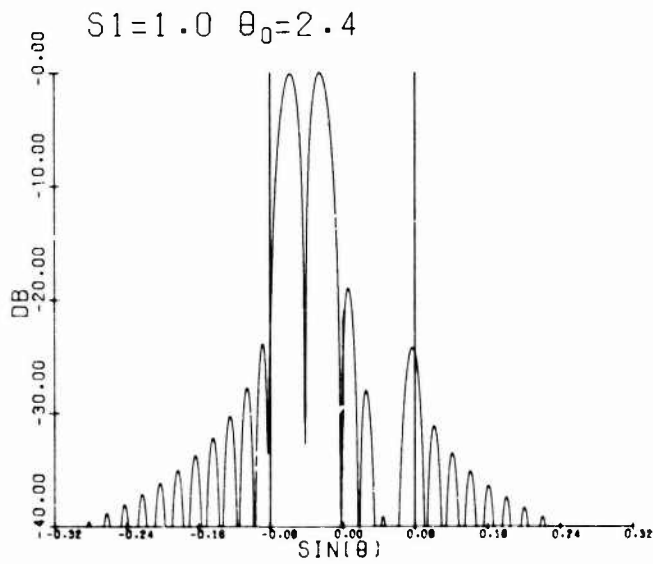


Figure 20. Difference Pattern; Scan Angle  $\theta_0 = 2.4^\circ$ , Frequency  $f_0$

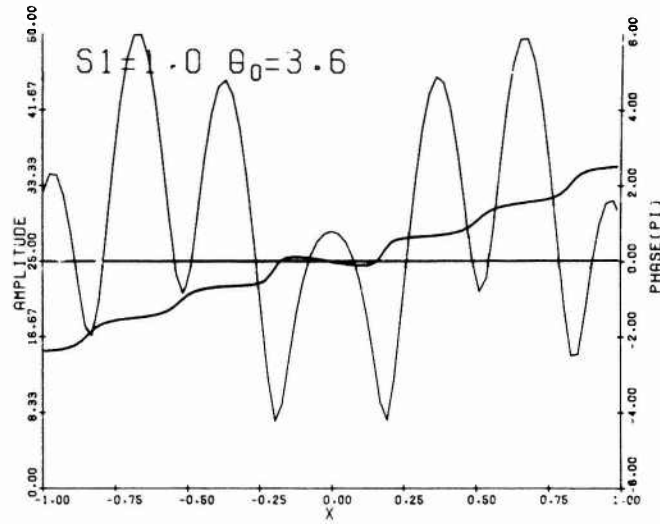


Figure 21. Difference Pattern, Amplitude and Phase Illumination; Scan Angle  $\theta_0 = 3.6^\circ$ , Frequency  $f_0$

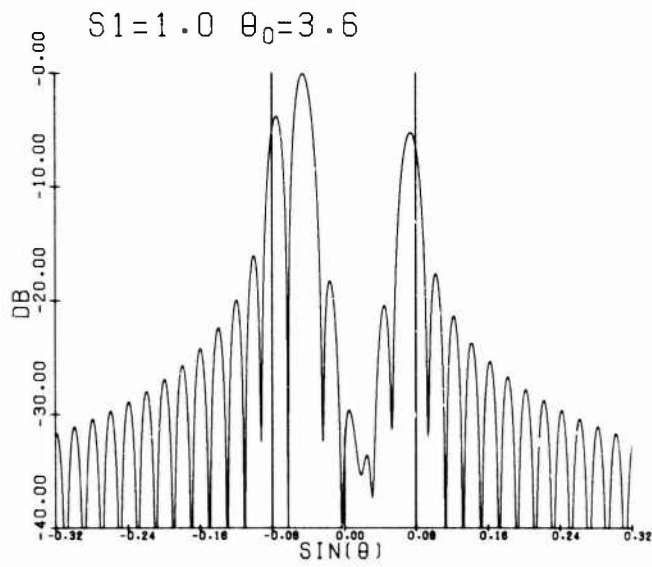


Figure 22. Difference Pattern; Scan Angle  $\theta_0 = 3.6^\circ$ , Frequency  $f_0$

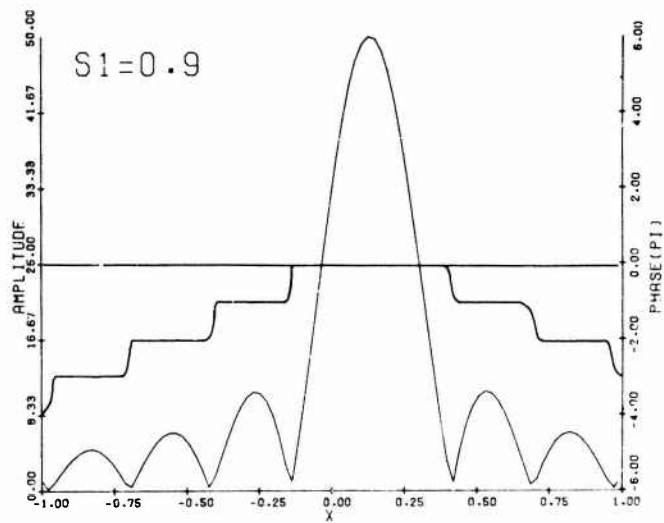


Figure 23. Amplitude and Phase Illumination of Subarray 1R, Frequency  $0.9 f_0$

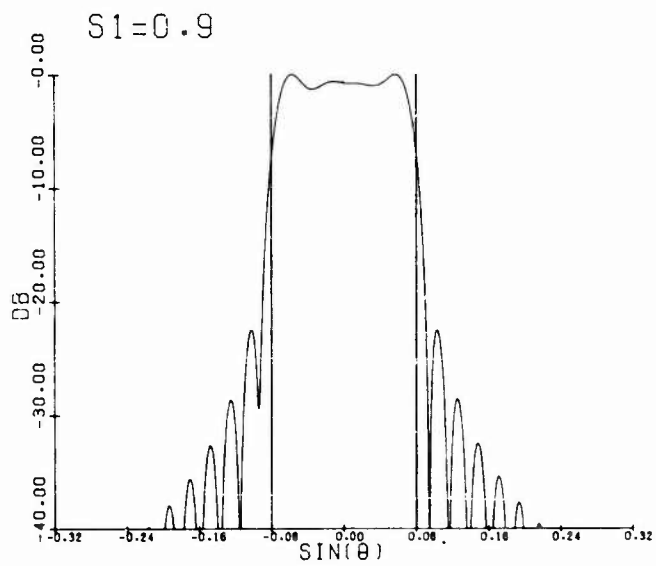


Figure 24. Radiation Pattern of Subarray 1R, Frequency  $0.9 f_0$

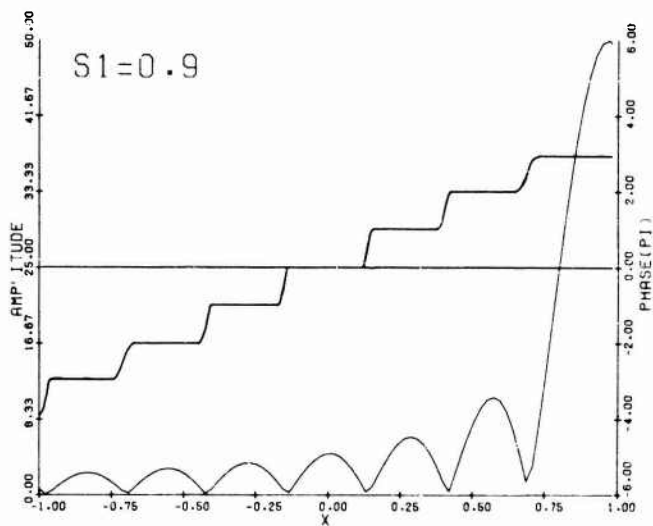


Figure 25. Amplitude and Phase Illumination of Subarray 4R, Frequency  $0.9 f_0$

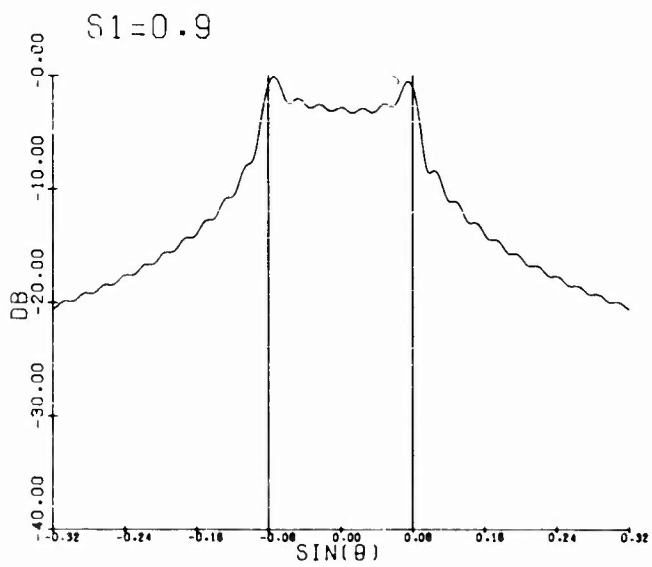


Figure 26. Radiation Pattern of Subarray 4R, Frequency  $0.9 f_0$

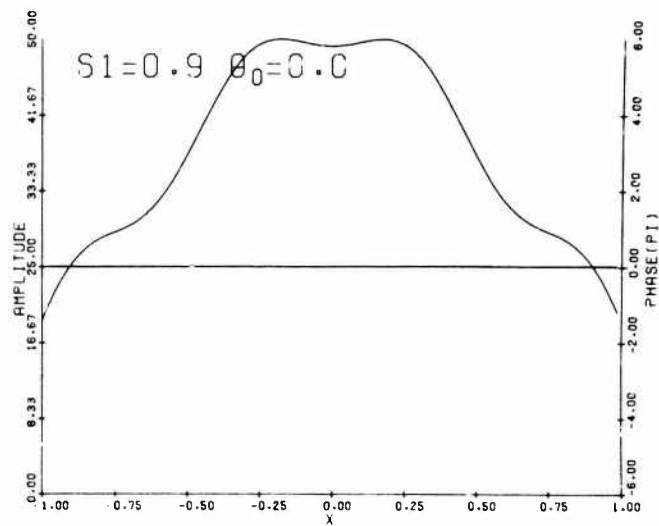


Figure 27. Sum Pattern, Amplitude and Phase Illumination; Scan Angle  $\theta_0 = 0^\circ$ , Frequency  $0.9 f_0$

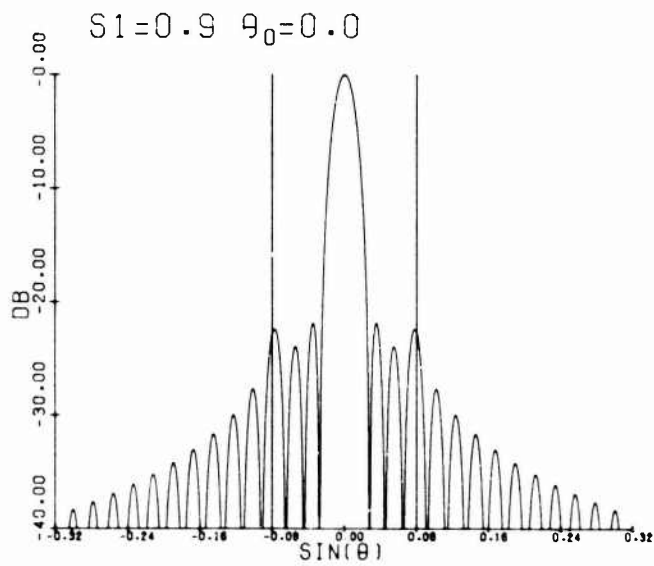


Figure 28. Sum Pattern; Scan Angle  $\theta_0 = 0^\circ$ , Frequency  $0.9 f_0$

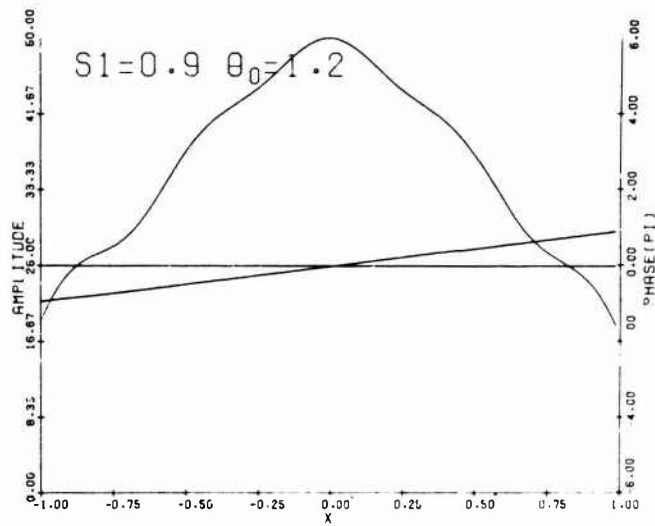


Figure 29. Sum Pattern, Amplitude and Phase Illustration; Scan Angle  $\theta_0 = 1.2^\circ$ , Frequency  $0.9 f_0$

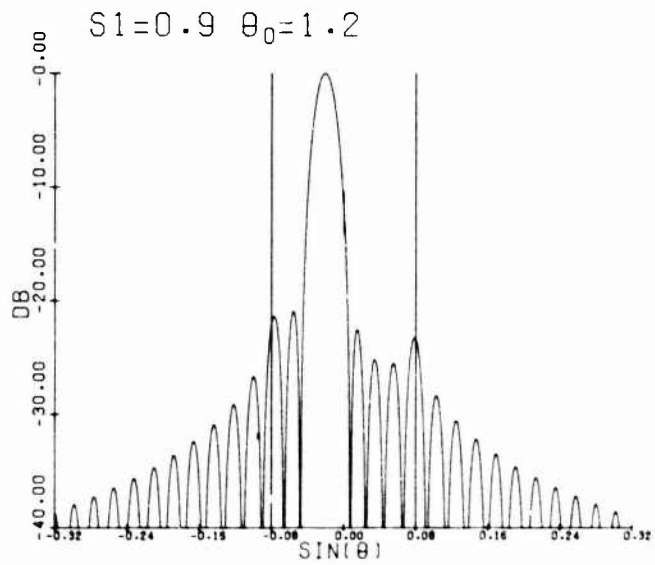


Figure 30. Sum Pattern; Scan Angle  $\theta_0 = 1.2^\circ$ , Frequency  $0.9 f_0$

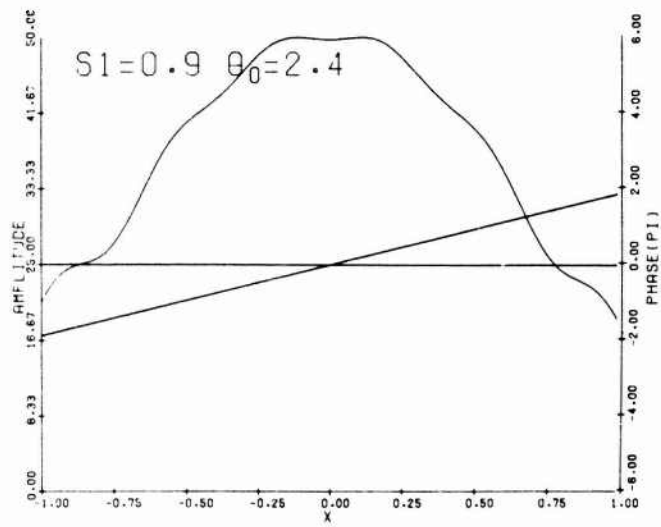


Figure 31. Sum Pattern, Amplitude and Phase Illumination; Scan Angle  $\theta_0 = 2.4^\circ$ , Frequency  $0.9 f_0$

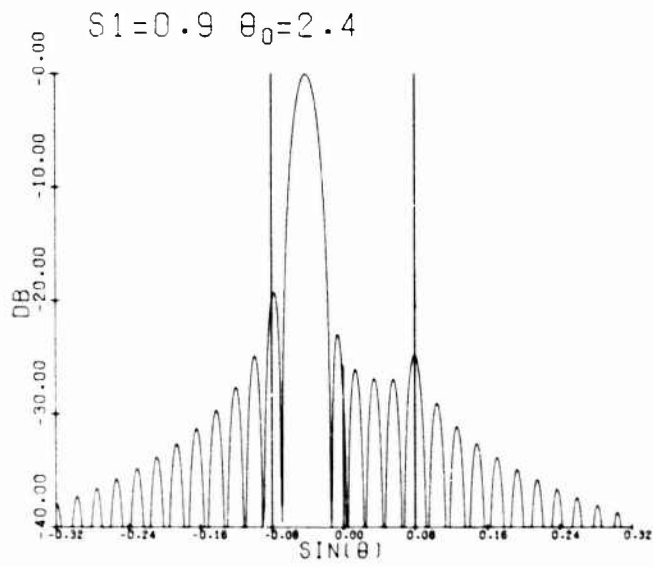


Figure 32. Sum Pattern; Scan Angle  $\theta_0 = 2.4^\circ$ , Frequency  $0.9 f_0$

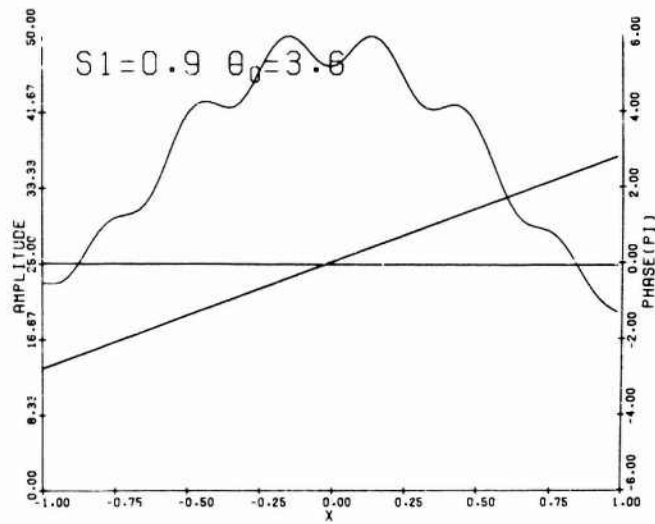


Figure 33. Sum Pattern, Amplitude and Phase Illumination; Scan Angle  $\theta_0 = 3.6^\circ$ , Frequency  $0.9 f_0$

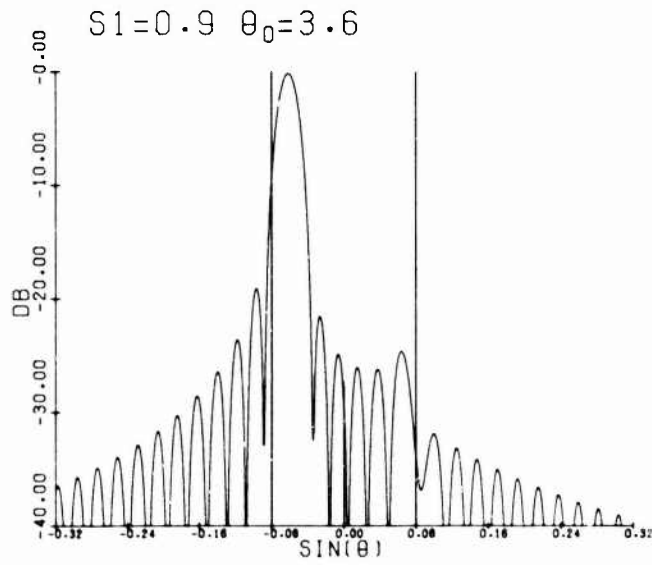


Figure 34. Sum Pattern; Scan Angle  $\theta_0 = 3.6^\circ$ , Frequency  $0.9 f_0$

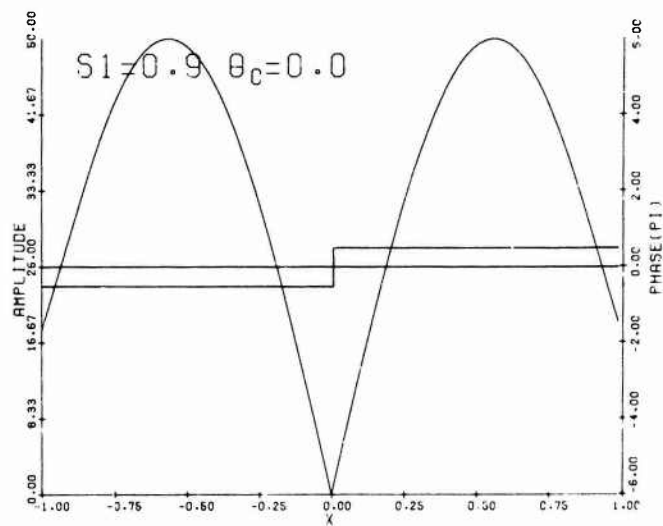


Figure 35. Difference Pattern, Amplitude and Phase Illumination; Scan Angle  $\theta_0 = 0^\circ$ , Frequency  $0.9 f_0$

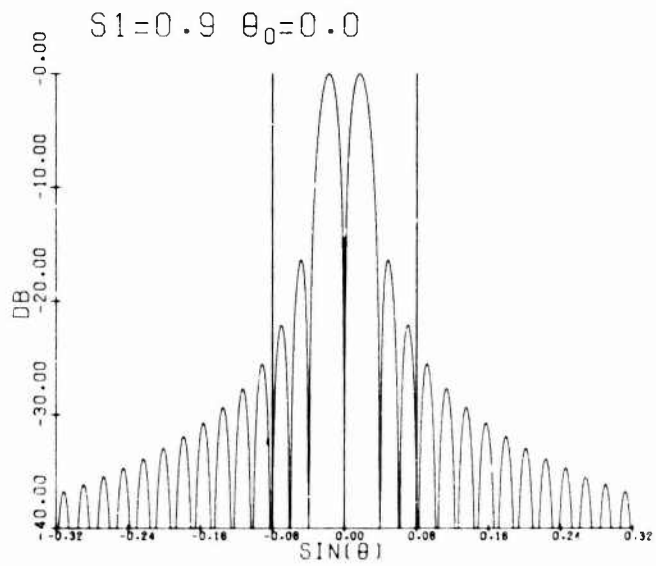


Figure 36. Difference Pattern; Scan Angle  $\theta_0 = 0^\circ$ , Frequency  $0.9 f_0$

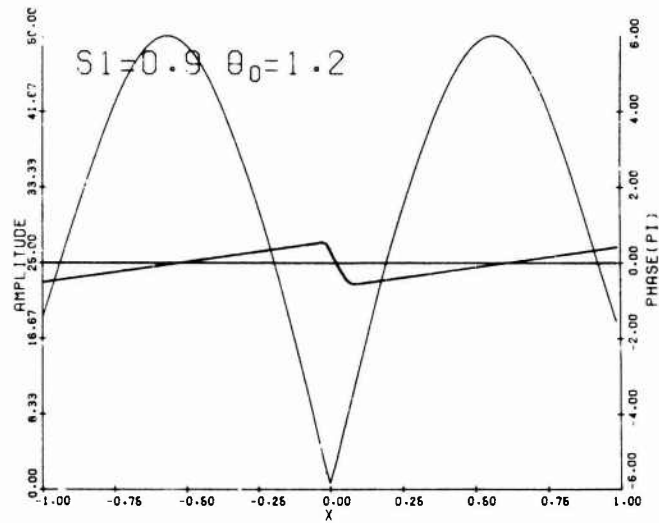


Figure 37. Difference Pattern, Amplitude and Phase Illumination; Scan Angle  $\theta_0 = 1.2^\circ$ , Frequency  $0.9 f_0$

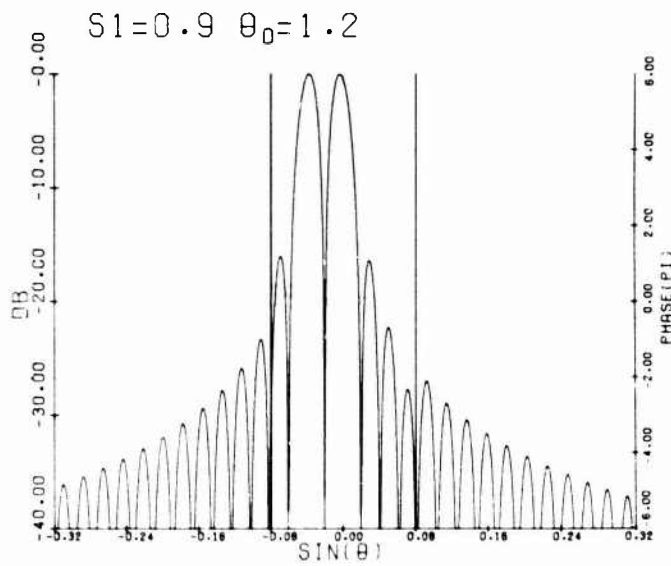


Figure 38. Difference Pattern; Scan Angle  $\theta_0 = 1.2^\circ$ , Frequency  $0.9 f_0$

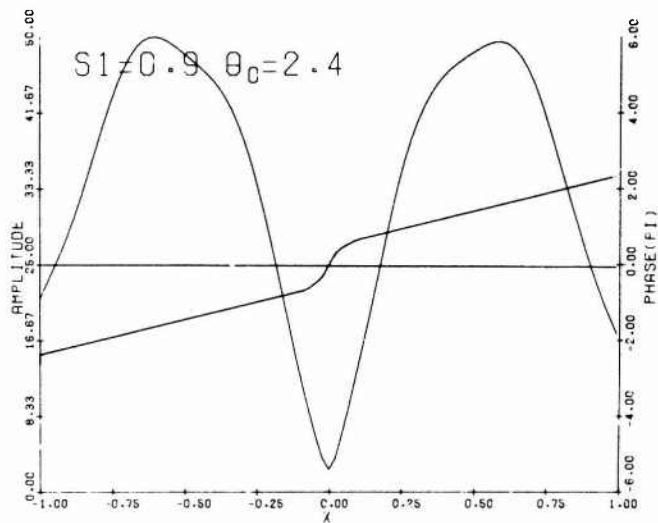


Figure 39. Difference Pattern, Amplitude and Phase Illumination; Scan Angle  $\theta_0 = 2.4^\circ$ , Frequency  $0.9 f_0$

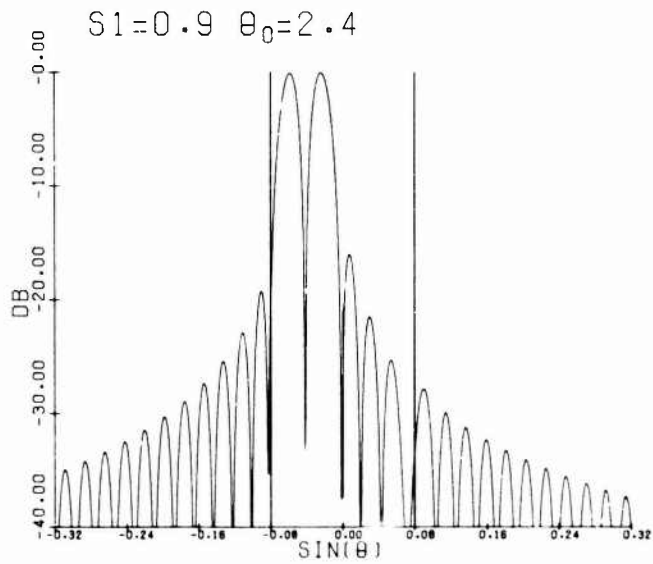


Figure 40. Difference Pattern; Scan Angle  $\theta_0 = 2.4^\circ$ , Frequency  $0.9 f_0$

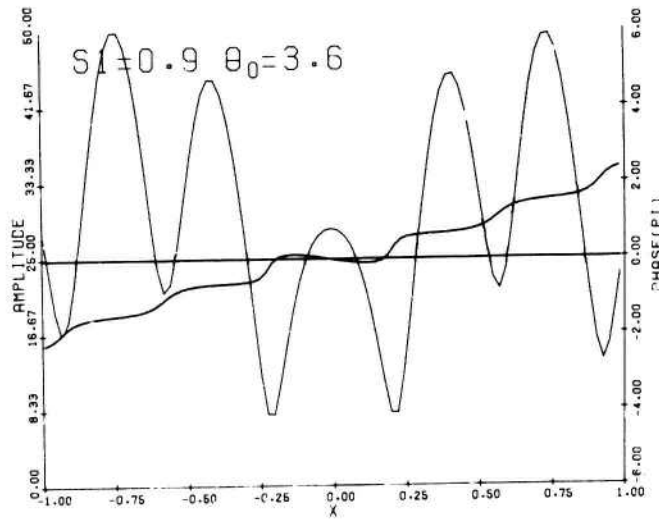


Figure 41. Sum Pattern, Amplitude and Phase Illumination; Scan Angle  $\theta_0 = 3.6^\circ$ , Frequency  $0.9 f_0$

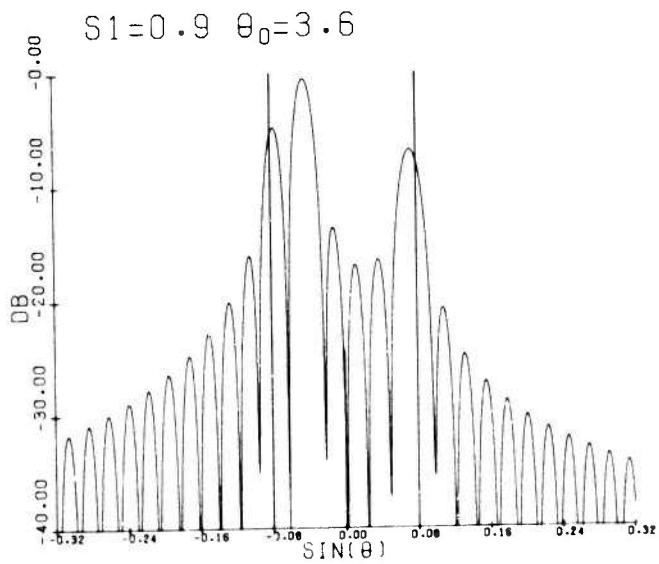


Figure 42. Difference Pattern; Scan Angle  $\theta_0 = 3.6^\circ$ , Frequency  $0.9 f_0$

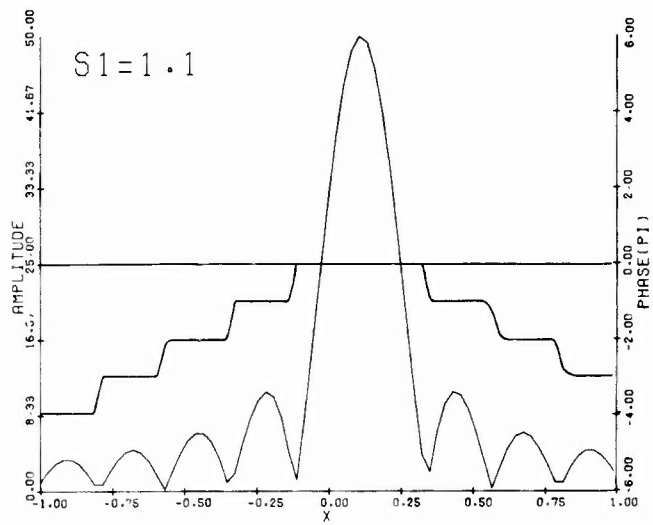


Figure 43. Amplitude and Phase Illumination of Subarray 1R, Frequency  $1.1 f_0$

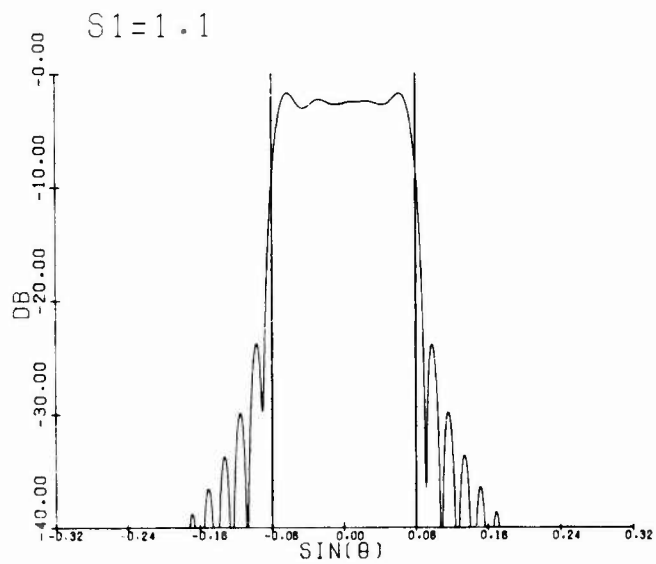


Figure 44. Radiation Pattern of Subarray 1R, Frequency  $1.1 f_0$

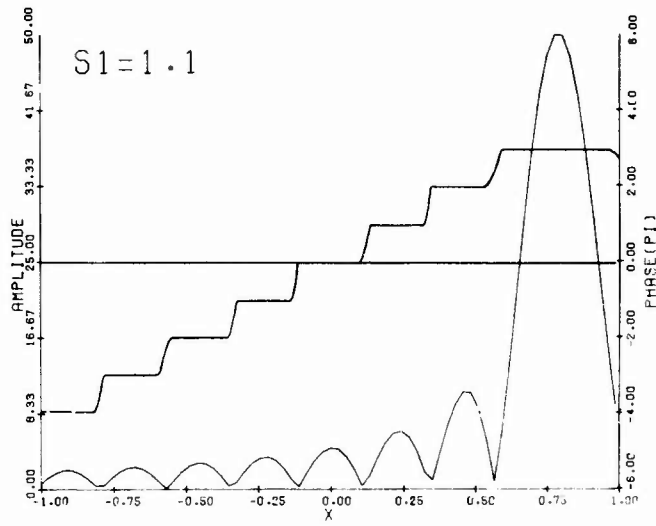


Figure 45. Amplitude and Phase Illumination of Subarray 4R, Frequency  $1.1 f_0$

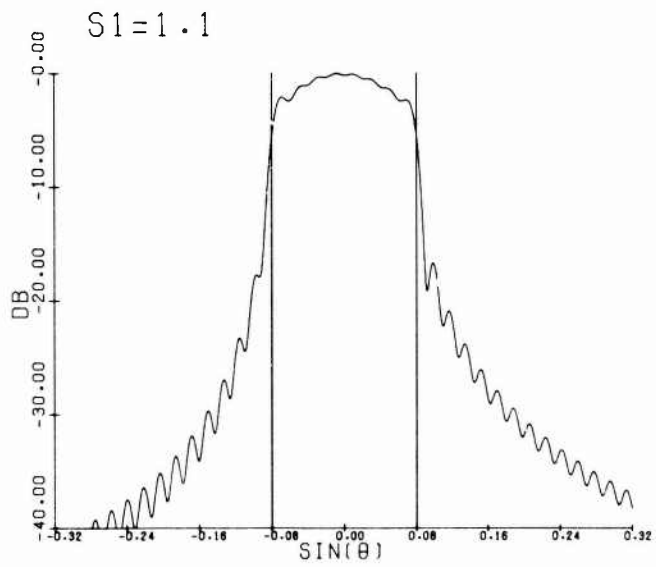


Figure 46. Radiation Pattern of Subarray 4R, Frequency  $1.1 f_0$

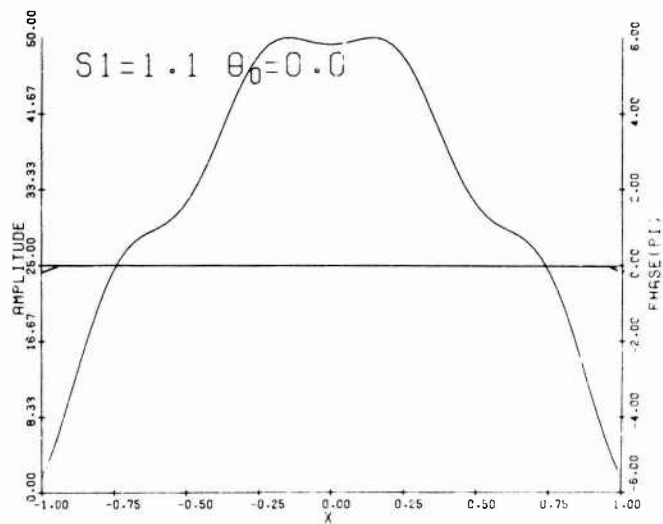


Figure 47. Sum Pattern, Amplitude and Phase Illumination; Scan Angle  $\theta_0 = 0^\circ$ , Frequency  $1.1 f_0$

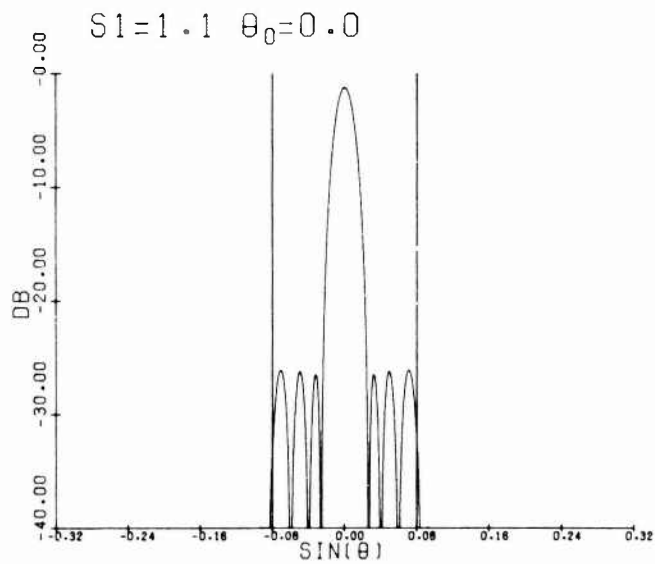


Figure 48. Sum Pattern; Scan Angle  $\theta_0 = 0^\circ$ , Frequency  $1.1 f_0$

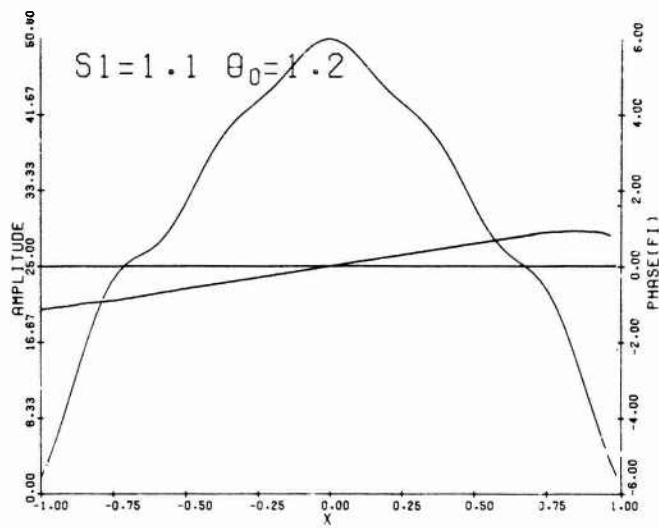


Figure 49. Sum Pattern, Amplitude and Phase Illumination; Scan Angle  $\theta_0 = 0^\circ$ , Frequency  $1.1 f_0$

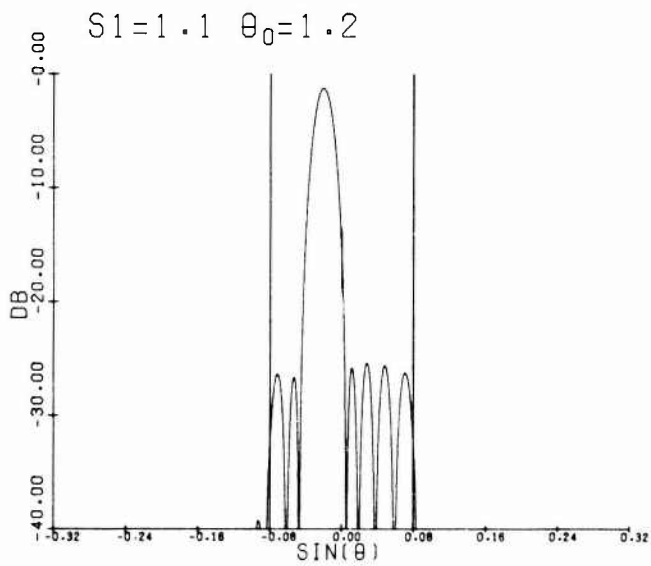


Figure 50. Sum Pattern; Scan Angle  $\theta_0 = 1.2^\circ$ , Frequency  $1.1 f_0$

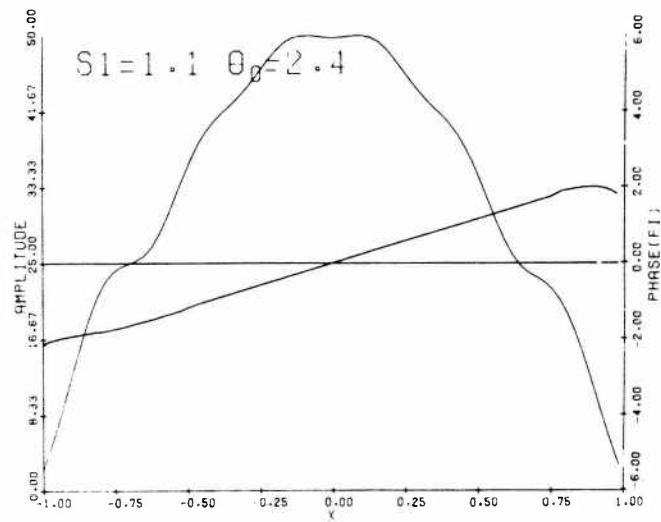


Figure 51. Sum Pattern, Amplitude and Phase Illumination; Scan Angle  $\theta_0 = 2.4^\circ$ , Frequency  $1.1 f_0$

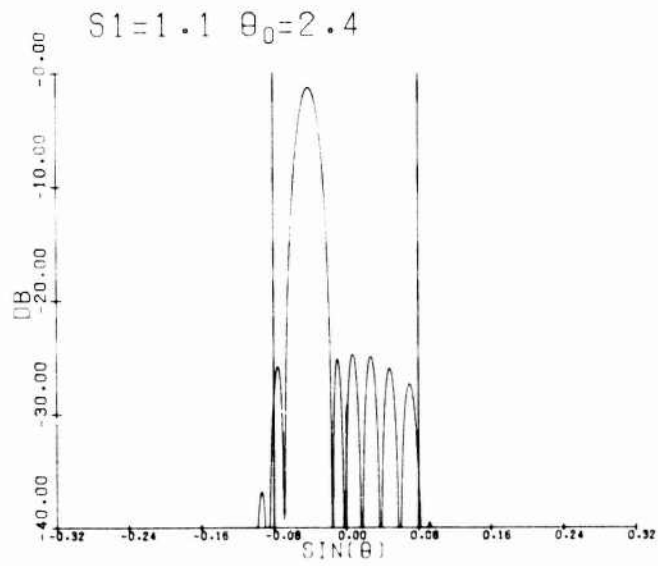


Figure 52. Sum Pattern; Scan Angle  $\theta_0 = 2.4^\circ$ , Frequency  $1.1 f_0$

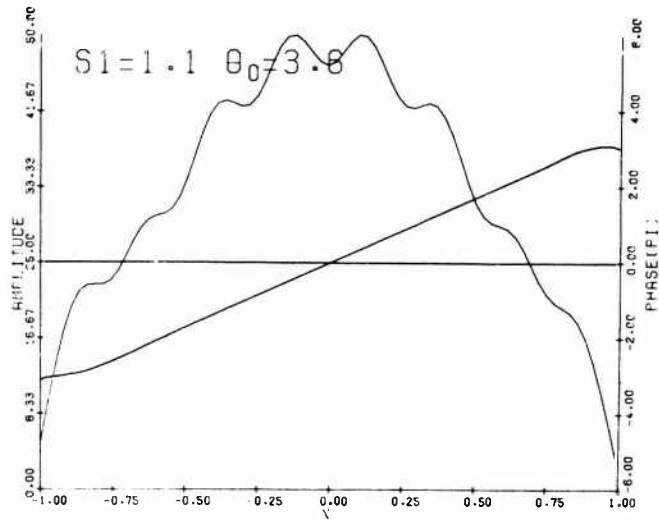


Figure 53. Sum Pattern, Amplitude and Phase Illustration; Scan Angle  $\theta_0 = 3.6^\circ$ , Frequency  $1.1 f_0$

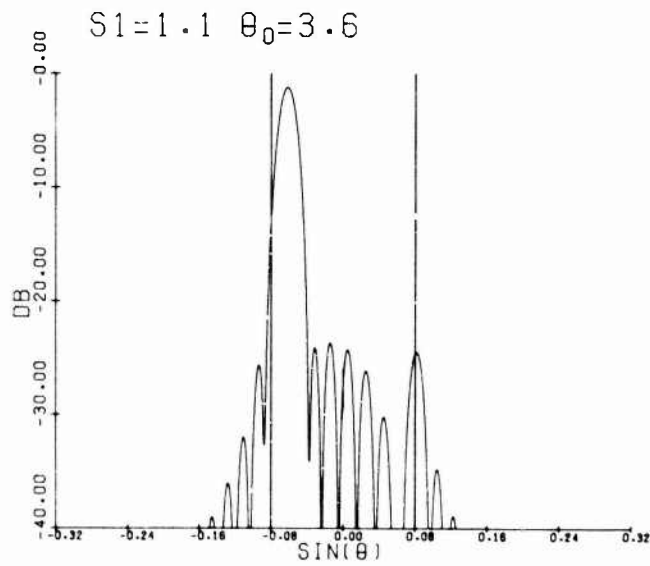


Figure 54. Sum Pattern; Scan Angle  $\theta_0 = 3.6^\circ$ , Frequency  $1.1 f_0$

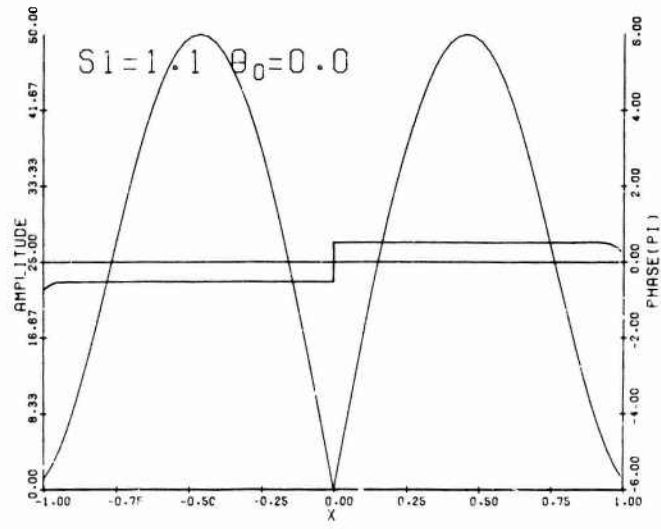


Figure 55. Difference Pattern, Amplitude and Phase Illumination, Scan Angle  $\theta_0 = 0^\circ$ , Frequency  $1.1 f_0$

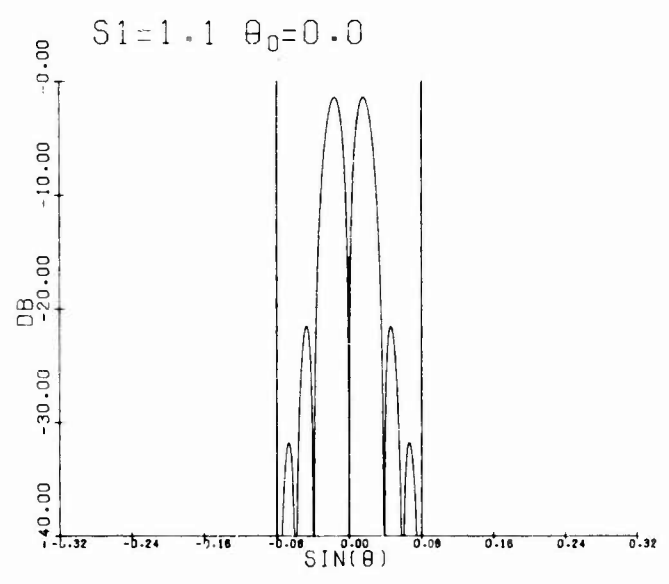


Figure 56. Difference Pattern; Scan Angle  $\theta_0 = 0^\circ$ , Frequency  $1.1 f_0$

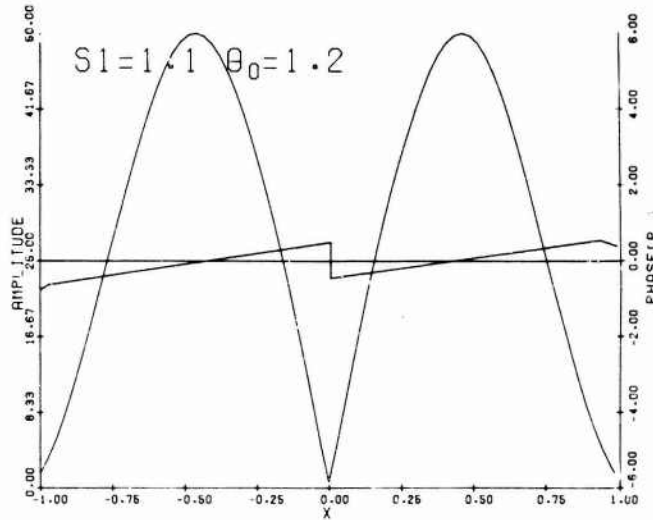


Figure 57. Difference Pattern, Amplitude and Phase Illumination; Scan Angle  $\theta_0 = 1.2^\circ$ , Frequency  $1.1 f_0$

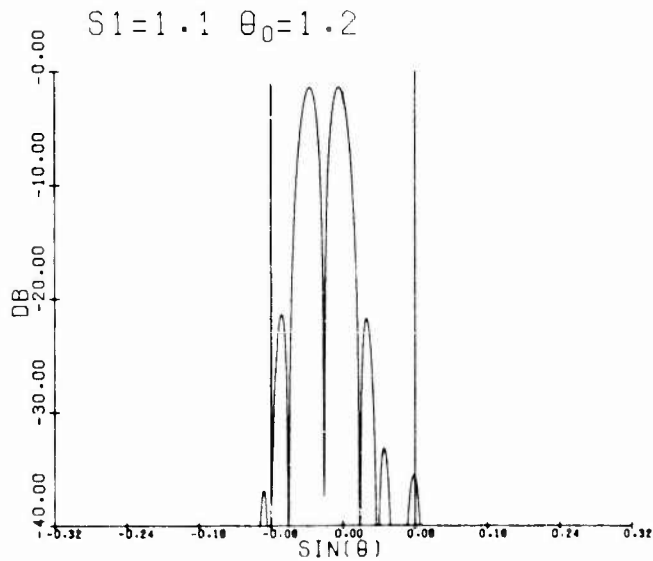


Figure 58. Difference Pattern; Scan Angle  $\theta_0 = 1.2^\circ$ , Frequency  $1.1 f_0$

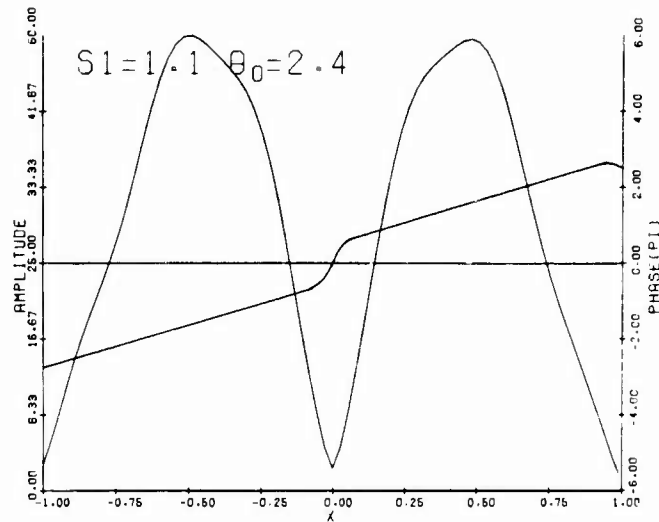


Figure 59. Difference Pattern, Amplitude and Phase Illumination; Scan Angle  $\theta_0 = 2.4^\circ$ , Frequency  $1.1 f_0$

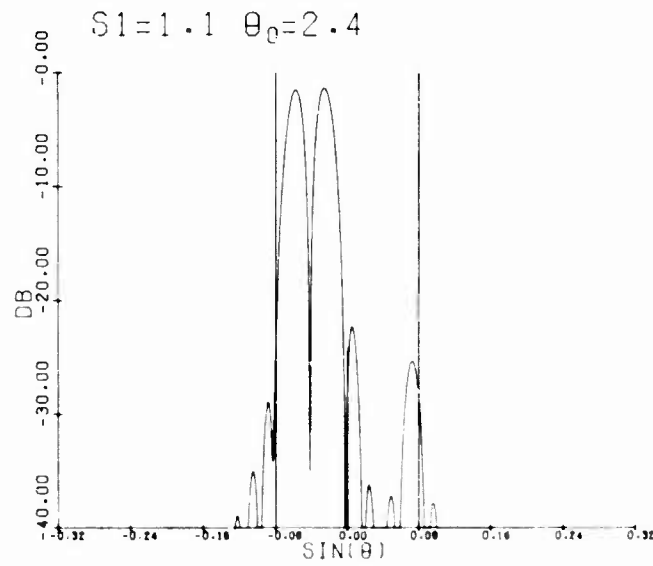


Figure 60. Difference Pattern; Scan Angle  $\theta_0 = 2.4^\circ$ , Frequency  $1.1 f_0$

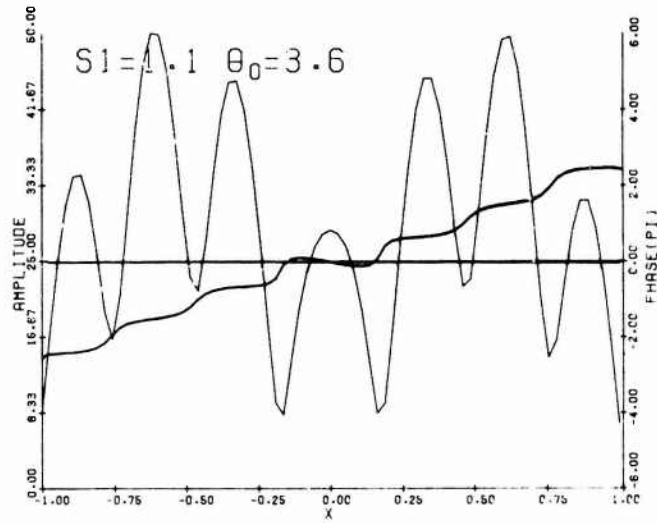


Figure 61. Difference Pattern, Amplitude and Phase Illumination; Scan Angle  $\theta_0 = 3.6^\circ$ , Frequency  $1.1 f_0$

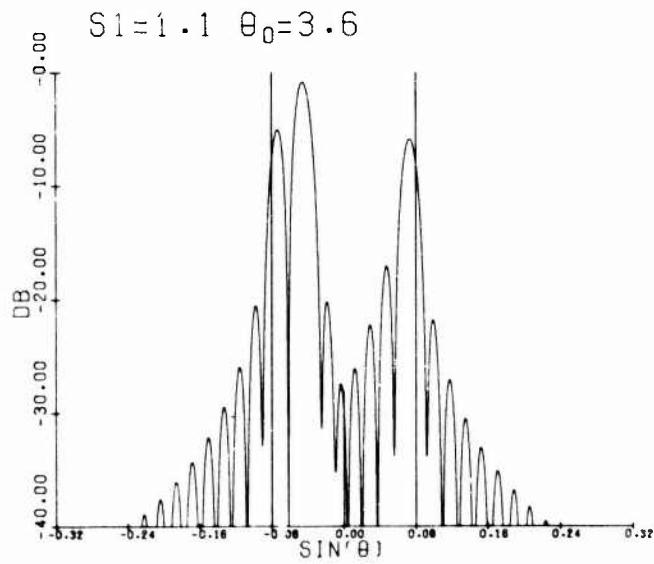


Figure 62. Difference Pattern; Scan Angle  $\theta_0 = 3.6^\circ$ , Frequency  $1.1 f_0$

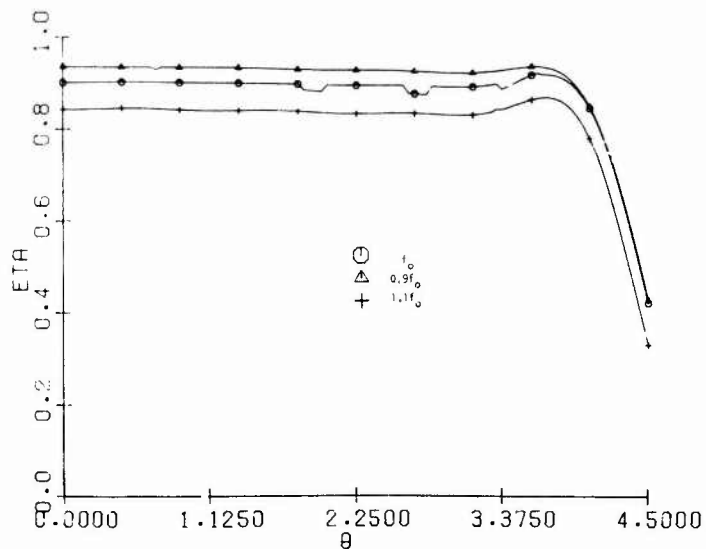


Figure 63. Illumination Efficiency vs Scan Angle

## 7. CONCLUSIONS

In this study a design scheme for an antenna system for limited scan in one plane has been discussed, the design principles outlined, and the performance numerically investigated. The proposed system has the property that the beam pointing and the beamwidth remain approximately constant with moderate changes in frequency for a fixed setting of the variable phase shifters. Hence the system is wide band in the sense that its band limitations are dictated by the pertinent properties of the microwave components (radiating and collecting elements, hybrid junctions, phase shifters, BFN) rather than by the overall antenna configuration and geometry. The number of phase shifters used in the scheme is close to the minimum theoretically possible, given by the product aperture in wavelengths by FOV in  $\sin\theta$  units. Calculated patterns indicated excellent performance expected.

The study performed refers to a 3 dB beamwidth of  $1.2^\circ$  and a FOV whose width is approximately 7 beamwidths. The specification of wider scan sector may lead to problems in designing suitable HN's. Since, however, the purpose of the HN is that of performing a spatial Fourier Transformation, the HN can possibly be replaced by a small lens in the focal region, performing, although only approximately, the same operation. This is a very interesting area of future investigation, because of the design flexibility and greater simplification achievable in this way. Also it seems that for the extension of the design scheme here proposed to two dimensional scan (that is, to tridimensional structures), such an approach is more attractive than that of using cascading HN's and BFN's; an alternative possible approach.

In recent years, the idea has been proposed of implementing scan in a limited sector by generating what can be called a "virtual feed" whose location in the focal region of a lens constituting the antenna aperture is controlled.<sup>9</sup> This is obtained by using a small focal lens and focusing on it the radiation of a small phased array. The idea is that of "matching" as closely as possible the receive focal field with the virtual feed distribution. Through this scheme an illumination of the main aperture is obtained whose amplitude remains approximately constant when the beam steering direction is changed and whose phase distribution is ideally linear. In the system proposed here, however, the concept is different; the amplitude distribution on the focal array varies with scan condition, and so does also the main lens aperture distribution, as we have shown in our numerical calculations. In fact, it can be shown that as a consequence of the two cascading Fourier Transformations occurring in the system, the amplitude distribution on the focal array for a certain scan direction is similar in shape to that portion of the far field pattern belonging to the FOV. The discussion of this point will not be pursued here, but the pertinent numerical analysis (not reported here) corroborates this contention. Thus, all the focal aperture, not only a limited part of it, contributes to the lens illumination, constituting in fact an oversized feed with carefully controlled current distribution. This is an alternative way of explaining why the secondary lens distribution is so well synthesized, yielding the excellent performance calculated.

---

9. Tang, C.H., and Winter, C.F. (1973) Study of the Use of a Phased Array to Achieve Pencil Beam over Limited Sector Scan, AFCRL-TR-73-048, ER73-4192, Raytheon Co., Final Report Contract F19628-72-C-0213.

## References

1. Mailloux, R. J., and Blacksmith, P. (1974) Array and reflector techniques for airport precision approach radars, Microwave J., pp 35-38.
2. Winter, C. (1968) Phase scanning experiments with two reflector antenna systems, Proc. IEEE 56(No. 11).
3. Schell, A. C. (1972) A Limited Sector Scanning Antenna, IEEE G-AP International Symposium.
4. Rudge, A. W., and Withers, M. J. (1971) New techniques for beam steering with fixed parabolic reflectors, Proc. IEE (British) 118(No. 7):857-863.
5. Tang, R. (1972) Survey of Time-Delay Beam Steering Techniques, Proc. 1970 Phased Array Antenna Symp., Artech House, pp 254-260.
6. Borgiotti, G. V. (1975) Degrees of Freedom of an Antenna Scanned in a Limited Sector, IEEE G-AP International Symp, pp 319-320.
7. Stark, L. (1974) Microwave theory of phased array antennas—a review, Proc. IEEE 62(No. 12):1661-1701.
8. Taylor, T. T. (1955) Design of line source antennas for narrow beamwidth and low sidelobes, IRE Tran. AP-3:16-28.
9. Tang, C. H., and Winter, C. F. (1973) Study of the Use of a Phased Array to Achieve Pencil Beam over Limited Sector Scan, AFCRL-TR-73-0482, ER73-4192, Raytheon Co., Final Report Contract F19628-72-C-0213.
10. Foster, H. E., and Hiatt, R. E. (1970) Butler network extension to any number of antenna ports, IEEE Transactions on Antennas and Prop. AP-18:818-820.
11. Lo, Y. T. (1964) A probabilistic approach to the problem of large antenna arrays, Radio Science 68D(No. 9):1011-1019.

## Appendix A

### A Hybrid Network with a Number of Input Ports Twice the Number of Output Ports

In designing antenna systems, it may prove necessary to design a hybrid matrix having a number of output (antenna) ports greater than the number of input (equipment) ports while still preserving beam orthogonality and high crossover levels for adjacent beams. The question of extending the Butler network scheme to any number of antenna ports was studied by Foster and Hiatt.<sup>10</sup> However, their solution leads to adjacent beams having low crossover levels. This is because in their work the number of output elements of a conventional  $N \times N$  Butler matrix is increased, through a particular design scheme, still keeping unchanged the relative phase difference between two adjacent output elements for each input excitation.

With the order  $N$  of a Butler matrix given, the maximum length of the aperture (that is, the minimum width of a beam) is determined by the need of limiting the element size to avoid grating lobes. Hence if one wants to generate  $N$  orthogonal beams having gains higher than those dictated by such a limitation with high crossover levels, one must resort to a more complex structure. A possible solution consists of using a Butler matrix of order  $2N \times 2N$ , and exciting only those  $N$  input ports generating the beams pointing into the directions closer to broadside. An alternative solution using two  $N$  order Butler matrices is here presented.

10. Foster, H. E., and Hiatt, R. E. (1970) Butler network extension to any number of antenna ports, IEEE Transactions on Antennas and Prop. AP-18:818-820.

Consider a Butler  $N \times N$  matrix,  $N$  being the even number of input and output ports, indexed by  $i$  and  $p$  respectively with  $i$  and  $p$  taking half integer values:

$$i, p = -\frac{N-1}{2}, -\frac{N-1}{2} + 1, \dots, \frac{N-1}{2}. \quad (\text{A1})$$

When the input port  $i$  is excited, the output voltages at the ports  $p$  can be represented by the set of  $N$  numbers

$$e_p(N|i) = N^{-1/2} \exp\left(jip \frac{2\pi}{N}\right), \quad (\text{A2})$$

where the indexes  $i, p$  can take all the values of Eq.(A1).

By using two identical  $N \times N$  Butler matrices with interlaced output elements and suitable connections of the input ports, we want to obtain a hybrid network generating a set of output voltages,

$$e_k(2N|i) = (2N)^{-1/2} \exp\left(jik \frac{\pi}{N}\right) \quad (\text{A3})$$

where  $i$ , the index of the input ports, takes the values of Eq.(A1) and the index  $k$  of the antenna ports takes the  $2N$  half integer values

$$k = -\frac{2N-1}{2}, -\frac{2N-1}{2} + 1, \dots, \frac{2N-1}{2}. \quad (\text{A4})$$

A way to achieve this result is the following. Let us consider the outputs of the component matrices A and B to be geometrically interlaced as in Figure 64. Output elements of the two matrices with the same indexes  $p$  [see Eq.A1)] are adjacent. Equal lengths of transmission lines connect the outputs of the component Butler matrices and the radiating elements. Corresponding input ports of the two matrices (that is, with the same index  $i$ ) are fed from a common input by dividing the power into two equal parts and using equal lengths of cables. However, two fixed phase shifters are inserted in front of corresponding input ports of the component matrices A and B. The phases inserted are, for the matrix A (Figure 64),

$$\phi_A(i) = \frac{\pi}{2N} i,$$

a delay or a lead according to the sign of  $i$ , and for the matrix B

$$\phi_B(i) = -\phi_A(i).$$

Thus the phase sequence at the output of the composite hybrid network will be for excitation of the port  $i$ ,

$$-\frac{2N-1}{2} i \frac{\pi}{N}, \left(-\frac{2N-1}{2} + 1\right) i \frac{\pi}{N}, \dots, \frac{2N-1}{2} i \frac{\pi}{N}$$

that is the set

$$\phi_{ik} = ik \frac{\pi}{N}$$

with  $k$  given by Eq. (A4). Thus the output voltages are identical to Eq. (A3) as sought.

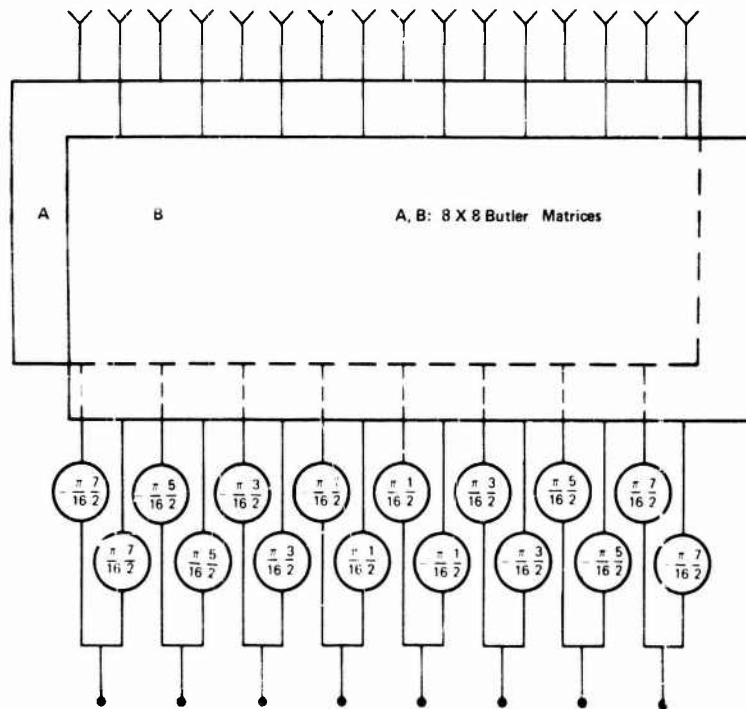


Figure 64. Composite Hybrid Network

## Appendix B

### The Effects of Phase Quantization on Radiation Pattern

It is well known that in a conventional array, with a phase shifter for each radiating element, the rms level of power associated with "hash radiation" due to phase errors is inversely proportional to the number of radiating elements and depends weakly upon the direction of observation (decaying with angle as the patterns of the radiating elements). For the design scheme proposed here the situation is different. In fact, the filtering effect of the subarray patterns reduces the rms sidelobe level to a negligible value at large angle from broadside. Only close-in sidelobes (within the FOV) are affected substantially by phase quantization. The following approximate analysis has the purpose of quantitatively defining the phenomenon and of providing a reasonable criterion for the determination of the number of bits to be used in the phase shifters for an assigned level of sidelobes.

Let us consider, for a certain direction  $u$ , the variance of the pattern, that is, the rms value of the difference between the pattern in absence of phase quantization error (namely, assuming analog, error-free phase shifters) and the pattern with the actual errors. We assume that the phase quantization errors of the various phase shifters are uncorrelated and uniformly distributed in the phase interval of the least significant bit. This implies that some form of "randomization" has been exploited, such as adding known, but randomly generated, fixed phase shifts to each subarray. We also assume that the phase error  $\gamma_p$  for subarray  $p$  is small. Thus we can write

$$\exp(j\gamma_p) \approx 1 + j\gamma_p \quad (B1)$$

Under these hypotheses the variance  $\sigma^2(u)$  of the pattern can be shown to be given by

$$\sigma^2(u) = E \left[ \left| \int_{-u_\epsilon}^{u_\epsilon} \sum_p a_p \gamma_p \exp \left( j p \pi \frac{\lambda - u_0}{u_\epsilon} \right) \frac{\sin a(u-\lambda)}{u-\lambda} d\lambda \right|^2 \right] \quad (B2)$$

where we recall that  $2a$  is the aperture length and where  $E[ \ ]$  is the statistical average operator. The phase errors are uncorrelated,

$$E[\gamma_p \gamma_q] = \delta_{pq} \sigma_\psi^2 \quad (B3)$$

where  $\delta_{pq}$  is the Kroneker's delta. For a phase shifter having  $B$  bits, the variance of the phase distribution is

$$\sigma_\psi^2 = \left( \frac{2\pi}{2^B} \right)^2 \frac{1}{12} . \quad (B4)$$

Because of Eq. (B3), the pattern variance takes the form,

$$\sigma^2(u) = \sum_p |a_p|^2 \sigma_\psi^2 \left| \int_{-u_\epsilon}^{u_\epsilon} \exp \left( j p \pi \frac{\lambda}{u_\epsilon} \right) \frac{\sin a(u-\lambda)}{u-\lambda} d\lambda \right|^2 \quad (B5)$$

independent of the scan direction. It is apparent that, unlike conventional arrays, the hash radiation is strongly angularly dependent and, outside the FOV, decays essentially as  $u^{-2}$ . This is, of course, due to the filtering effect of subarray patterns.

If we consider points  $u$  within the FOV no large error is committed if we replace in Eq. (B5)  $\sin au/u$  with  $1/\pi$  times a delta function. This is because for every well behaved function  $t(\lambda)$

$$\lim_{a \rightarrow \infty} \int t(\lambda) \frac{\sin a(u-\lambda)}{u-\lambda} d\lambda = \pi t(u) . \quad (B6)$$

Thus since  $a \gg 1/u_\epsilon$ , for  $u$  belonging to the FOV, we can write approximately

$$\sigma^2(u) \approx \sum_p |a_p|^2 \sigma_\psi^2 \pi^2 \quad \text{for } |u| < u_\epsilon \quad (B7)$$

independent of  $u$ .

In order to understand how the "hash radiation" [Eq. (B7)] affects the pattern, normalize it to the error-free power pattern on its peak, that is to

$$|g(u_0|\theta_0)|^2 = \left| \sum_p a_p \int_{-u_\epsilon}^{u_\epsilon} \exp\left(j\pi p \frac{\lambda - u_0}{u_\epsilon}\right) \frac{\sin a(u_0 - \lambda)}{u_0 - \lambda} d\lambda \right|^2. \quad (B8)$$

Following the same reasoning leading from Eq. (B5) to Eq. (B7), we may write

$$|g(u_0|\theta_0)|^2 \simeq \left| \sum_p a_p \right|^2 \pi^2; \quad (B9)$$

thus

$$\frac{\sigma^2(u)}{|g_0(u_0|\theta_0)|^2} = \frac{\sum_p |a_p|^2 \sigma_\psi^2}{\left| \sum_p a_p \right|^2} \quad (B10)$$

or approximately

$$\frac{\sigma^2(u)}{|g_0(u_0|\theta_0)|^2} \simeq \frac{\sigma_\psi^2}{\eta N} \quad (B11)$$

where  $\eta$  is the efficiency of the illumination that has been approximated through sampling at the abscissae of the  $N$  subarray centers.

A way of specifying the number of the phase shifters is to require that Eq. (B11) be less than a chosen amount. For example, we may require that Eq. (B11) be one half the minimum nominal sidelobe level within the FOV. For the numerical case discussed in Section 5, we will require that Eq. (B11) be close to -28 dB, since in the FOV all sidelobes are nominally -25 dB under the peak. This yields for  $N=8$ ,  $\eta=0.9$  [from Eq. (B11)]

$$\sigma_\psi^2 = 0.0114 \text{ rad}^2. \quad (B12)$$

From Eq. (B4), if  $B$  is chosen equal to 4, one finds

$$\sigma_\psi^2 = 0.0128 \text{ rad}^2 \quad (B13)$$

that is close enough to the value (B12).

The criterion which has been used here to determine the number of bits of the phase shifters is, of course, somewhat arbitrary. A more systematic and

logical way consists of determining the probability density of the pattern for a given  $u$  and of establishing the level of confidence for a sidelobe not exceeding an assigned threshold. The philosophy underlying such an approach, has been outlined in Lo,<sup>11</sup> although for a different situation, and a discussion of the matter is outside the scope of this report.

---

11. Lo, Y. T. (1964) A probabilistic approach to the problem of large antenna arrays, Radio Science 68D(No. 9):1011-1019.